NASA TECHNICAL MEMORANDUM

NASA TM X- 73,195

NASA TM X- 73,195

A FLIGHT INVESTIGATION OF A 4D AREA NAVIGATION SYSTEM CONCEPT FOR STOL AIRCRAFT IN THE TERMINAL AREA

Frank Neuman, David N. Warner, and Francis J. Moran

Ames Research Center
Moffett Field, Calif. 94035

March 1977

1. Report No. NASA TM X-73,195	2. Government Accession No.	3. Recipient's Catalog No.
4. Title and Subtitle A FLIGHT INVESTIGATION OF A 4D AREA NAVIGATION SYSTEM CONCEPT FOR STOL AIRCRAFT IN THE TERMINAL AREA		5. Report Date 6. Performing Organization Code
7. Author(s) Frank Neuman, David N. Warner, and Francis J. Moran		8. Performing Organization Report No. A-6879 10. Work Unit No. 513-53-03
9. Performing Organization Name and Address NASA-Ames Research Center Moffett Field, Calif. 94035		11. Contract or Grant No. 13. Type of Report and Period Covered Technical Memorandum
12. Sponsoring Agency Name and Address National Aeronautics and Space Administration Washington, D.C. 20546		14. Sponsoring Agency Code
15. Supplementary Notes		

16 Abstract

A digital avionics system referred to as STOLAND has been test-flown in the NASA CV-340 aircraft to obtain performance data for time-controlled guidance in the manual flight director mode. The advanced system components installed in the cockpit included an electronic attitude director indicator and an electronic multifunction display. Navigation guidance and control computations were all performed on a digital computer. A detailed 4D area navigation systems description is given. The pilot/system interface and systems operation and performance are also described. Approach flightpaths were flown which included a 180° turn and a 1-min, 5° straight-in approach to 30-m altitude, at which point go-around was initiated. Results are presented for 19 approaches.

17. Key Words (Suggested by Author(s))	18. Distribution Statement		
Aircraft guidance 4D RNAV RNAV	Unlimited STAR Category - ~~21~~ 4		
19. Security Classif. (of this report) Unclassified	20. Security Classif. (of this page) Unclassified	21. No. of Pages 56	22. Price* $4.25

*For sale by the National Technical Information Service, Springfield, Virginia 22161

SYMBOLS

a_m, b_m	sin ψ_m, cos ψ_m, respectively, of bearing angle
A_i, B_i	coefficients defining phantom target position
d_m	distance along specified flightpath between waypoints m and n
d_{rng}	distance from aircraft to next waypoint measured along reference flightpath
D_m	velocity gradient ($\partial V/\partial s$) between waypoints m and n
g	acceleration of gravity
h_{err}	vertical deviation of aircraft from the reference flightpath
k_1, k_2	constants in lateral tracking control law
k_3, k_4, k_5	constants in vertical control law
k_6	constant in airspeed command signal control law
M_i, N_i	crosstrack and alongtrack wind components, respectively, at a waypoint
N_{acc}	aircraft acceleration normal to aircraft
R_m	radius of curvature of circular reference flightpath
S	alongtrack distance
S_i	phantom target position within a path segment
t_J	prescribed arrival time at critical waypoint
V_{AN}	prescribed nominal airspeed
V_{cref}	airspeed command signal
V_g	aircraft ground velocity
V_{GN}	nominal ground speed
V_w	wind estimate
V_{wx}, V_{wy}	filtered x and y components of V_w

$\hat{x},\hat{y},\hat{z}$	estimated aircraft position in a runway coordinate system
$\dot{\hat{x}},\dot{\hat{y}},\dot{\hat{z}}$	estimated ground speeds of aircraft in a runway coordinate system
x_m,y_m,z_m	coordinates of initial point of reference flightpath segment
$\hat{x}_n,\hat{y}_n,\hat{z}_n$	coordinates of terminal point of reference flightpath segment
x_R,z_R	circle center coordinates of aircraft in turn
y_{err}	lateral deviation of aircraft from reference flightpath
$\dot{y}$	crosstrack velocity
z_{err}	altitude error
α	angle between V_w and V_{AN}
ΔS	alongtrack distance from estimated aircraft position to desired aircraft position
Δt_i	time required to fly from waypoint i to waypoint i + 1
$\Delta\gamma$	predicted pitch maneuver or increment in flightpath angle
$\Delta\psi$	angle of turn of aircraft
γ_{err}	flightpath angle error
γ_I	inertial flightpath angle
γ_{ref_n}	nominal flightpath angle
ϕ_c	lateral cracking control command
ϕ_p	nominal roll angle
ψ_{cm},ψ_{cn}	initial and final bearings, respectively, of aircraft
θ_c	pitch command

A FLIGHT INVESTIGATION OF A 4D AREA NAVIGATION SYSTEM CONCEPT FOR STOL AIRCRAFT IN THE TERMINAL AREA

Frank Neuman, David N. Warner, and Francis J. Moran

Ames Research Center

SUMMARY

A digital avionics system referred to as STOLAND has been test-flown in the NASA CV-340 aircraft to obtain performance data for time-controlled guidance in the manual flight director mode. The advanced system components installed in the cockpit included an electronic attitude director indicator and an electronic multifunction display. Navigation guidance and control computations were all performed on a digital computer. A detailed 4D area navigation systems description is given. The pilot/system interface and systems operation and performance are also described. Approach flightpaths were flown which included a 180° turn and a 1-min, 5° straight-in approach to 30-m altitude, at which point go-around was initiated. Results are presented for 19 approaches.

INTRODUCTION

Studies have shown (e.g., refs. 1 and 2) that short-haul aircraft may provide an effective transportation system that can operate into city centers and suburban facilities. To provide the detailed data base required for the design and development of such a short-haul system, a joint DOT/NASA STOL Operating Systems Experiment Program has been initiated. As a part of this joint program, Ames Research Center has developed an experiments program with the overall objective of providing information that will aid in the choice of terminal area guidance, navigation, and control system concepts for short-haul aircraft, and in investigating operational procedures.

In a short-haul transportation system, various levels of avionics systems capability may be needed. Simple, low-cost systems may be adequate for navigation, guidance, and control of aircraft operating in low-density traffic conditions and relatively good weather. More complex and costly automated systems may be economically justifiable for operations in high-density traffic conditions and poor weather. The test data obtained in this program will provide a basis for the selection of system capability to meet operational requirements (e.g., runway requirements, weather minimums, etc.) and will also provide means for estimating the system acceptability and system cost.

A digital avionics system, referred to as STOLAND, has been installed (without servos) in the NASA CV-340 twin-engine transport aircraft. Nineteen test flights have been made to obtain preliminary STOLAND performance data

in the manual flight director mode using time-controlled guidance (i.e., 4D area navigation (4D RNAV)). STOLAND is also installed (with servos) in the powered-lift Augmentor Wing Jet STOL research aircraft (fig. 1) described in reference 3 and in a DeHavilland DHC-6 Twin Otter STOL aircraft. Reference 4 gives an overall functional description of all the STOLAND features for the three airplanes in which it was installed.

Investigations are being conducted in these aircraft to obtain performance data on both simple and sophisticated avionics system concepts, including autoland, and the corresponding STOL operating procedures. Reference 5 describes the technical details of the navigation system and the flight test results obtained in the CV-340. The navigation system was specifically designed to perform RNAV experiments at Crows Landing NALF, Crows Landing, Calif., which has TACAN and an experimental microwave landing system installed. Reference 6 describes the technical details and flight test results of the Ames-designed 4D RNAV system in the CV-340. This system included a timed capture trajectory and therefore was the first true 4D RNAV system. Reference 7 is a brief conference paper on the Sperry-designed 4D RNAV system flight test results in the CV-340. Reference 8 ties together the 4D RNAV experience to date and also includes some experience with automatic 4D RNAV in the Augmentor Wing Jet STOL research aircraft.

This report uses the same flight test data as reference 7, but examines them in detail. In particular, it distinguishes between left and right turning approaches, which brings out the importance of navigation bias errors on flightpath distortion. The second contribution of this report is the technical description of the 4D RNAV system.

SYSTEM DESCRIPTION

STOLAND is an integrated digital avionics system which performs all terminal area navigation, guidance, and automatic control functions for a STOL test vehicle along a curved reference approach flightpath. Included in the system are the autopilot modes considered standard for commercial transport aircraft and an autothrottle. The major components of the system are a Sperry 1819A general-purpose digital computer and a data adapter that interfaces all the navigation aids, displays, controls, and servo actuators (fig. 2). The navigation aids include VHF omnirange (VOR), distance measuring equipment (DME), tactical air navigation (TACAN), instrument landing system (ILS), microwave modular instrument landing system described in reference 9 (MODILS), and a radio altimeter.

The system components installed in the cockpit of the aircraft (fig. 3) include a horizontal situation indicator (HSI), an electronic attitude director indicator (EADI), a multifunction display (MFD), an MFD control panel, a mode select panel (MSP), a status panel, and a data entry panel. During automatic operation, the pilot monitors the system operation through the various cockpit displays. During flight director operation, the pilot uses the same set of displays to fly the aircraft along the reference

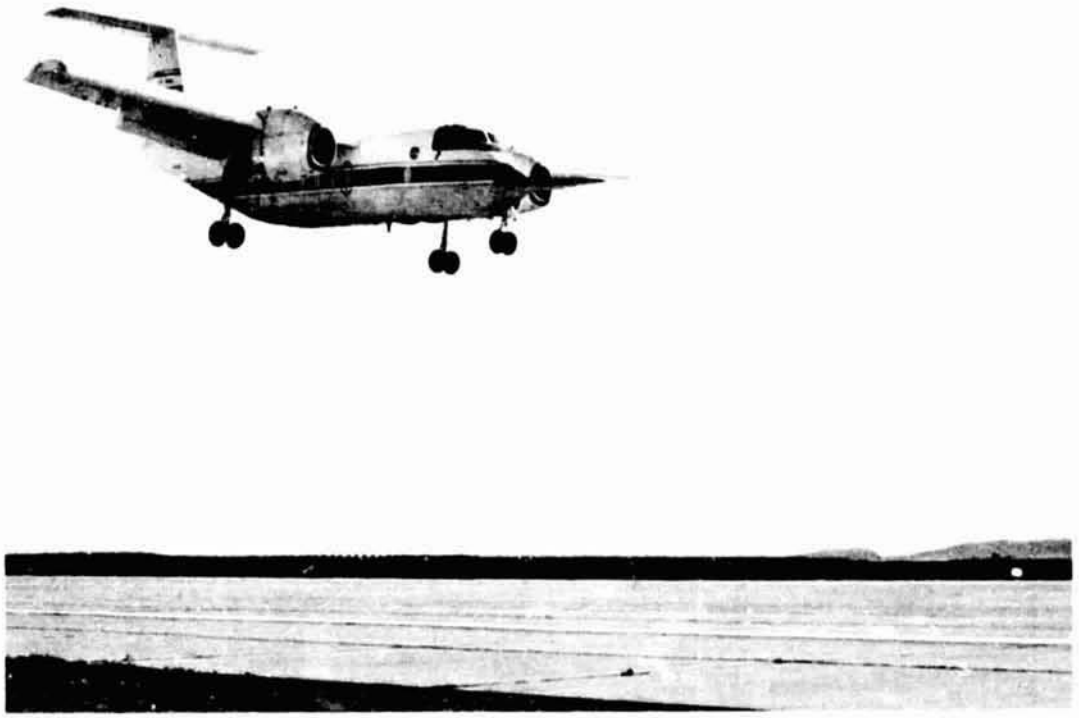

Figure 1.- Augmentor wing jet STOL research aircraft.

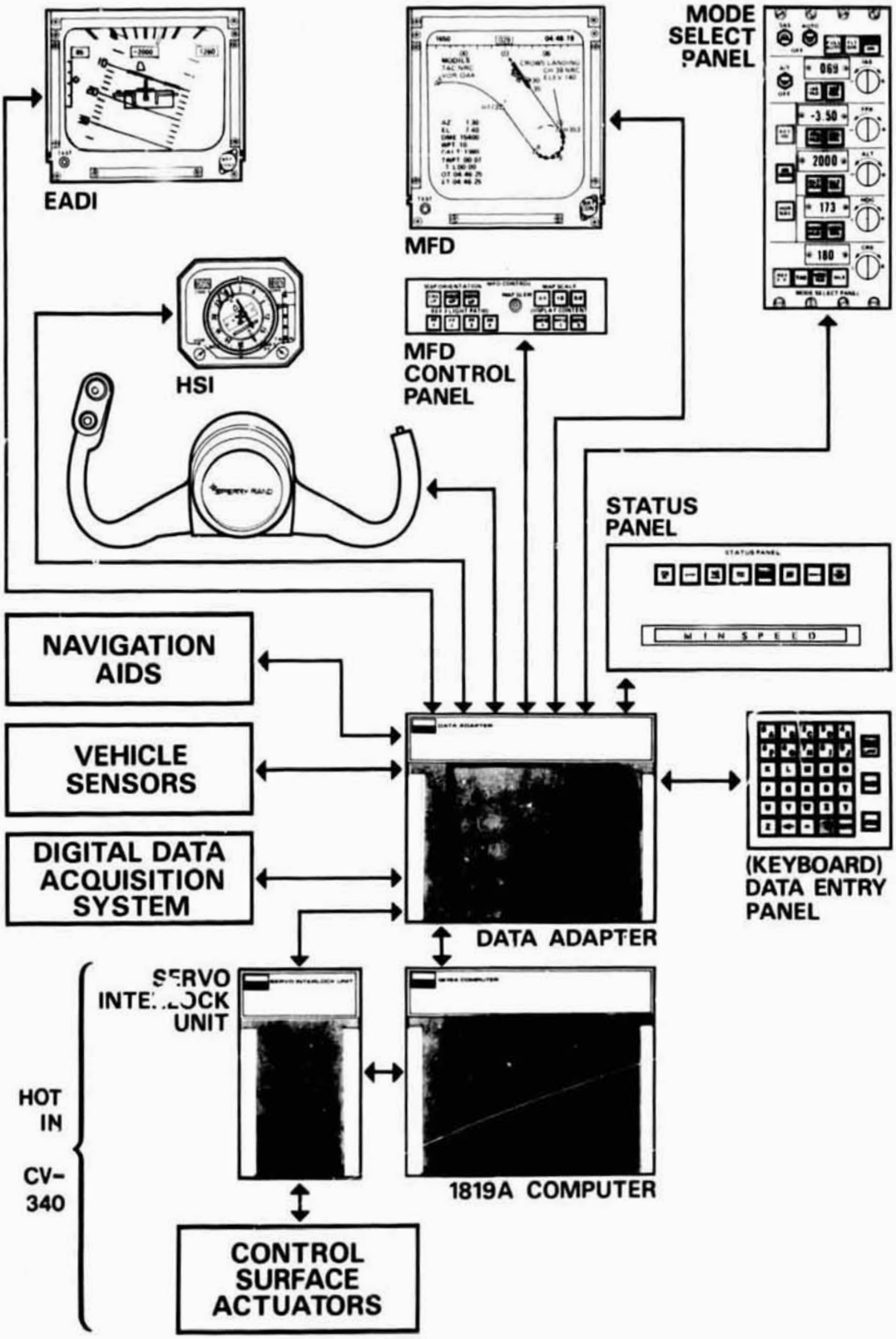

Figure 2.- STOLAND flight-test system.

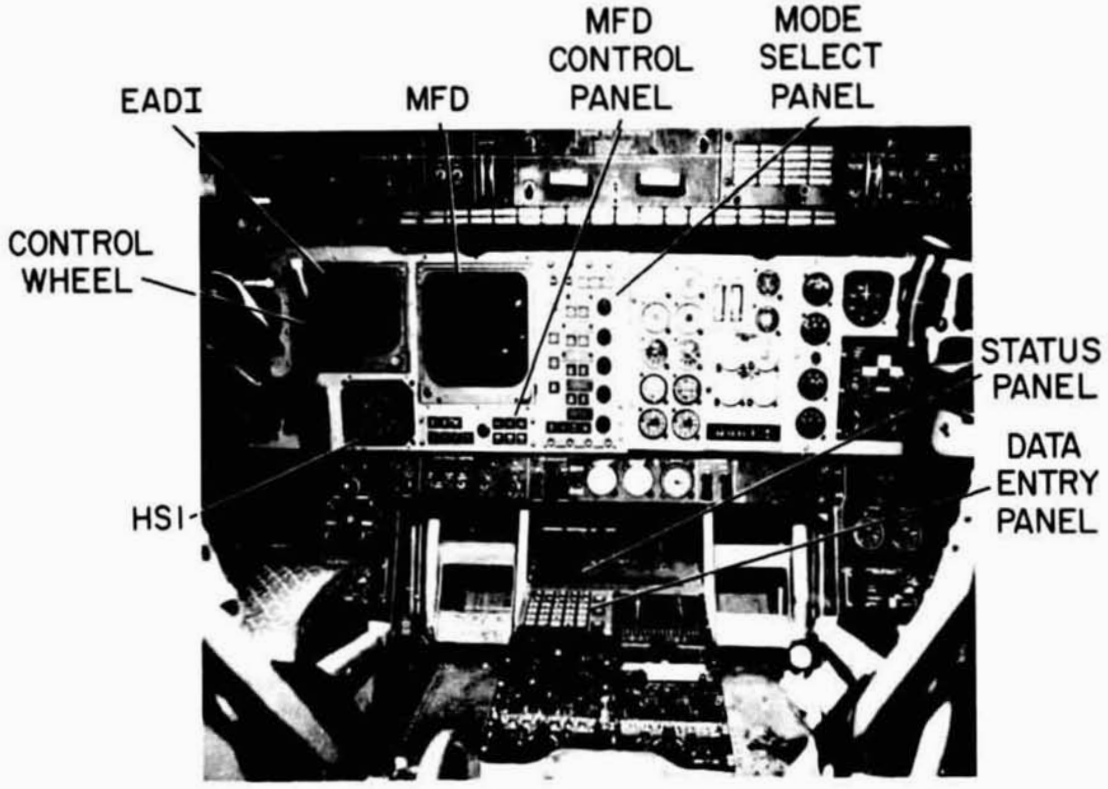

Figure 3.- STOLAND cockpit installation.

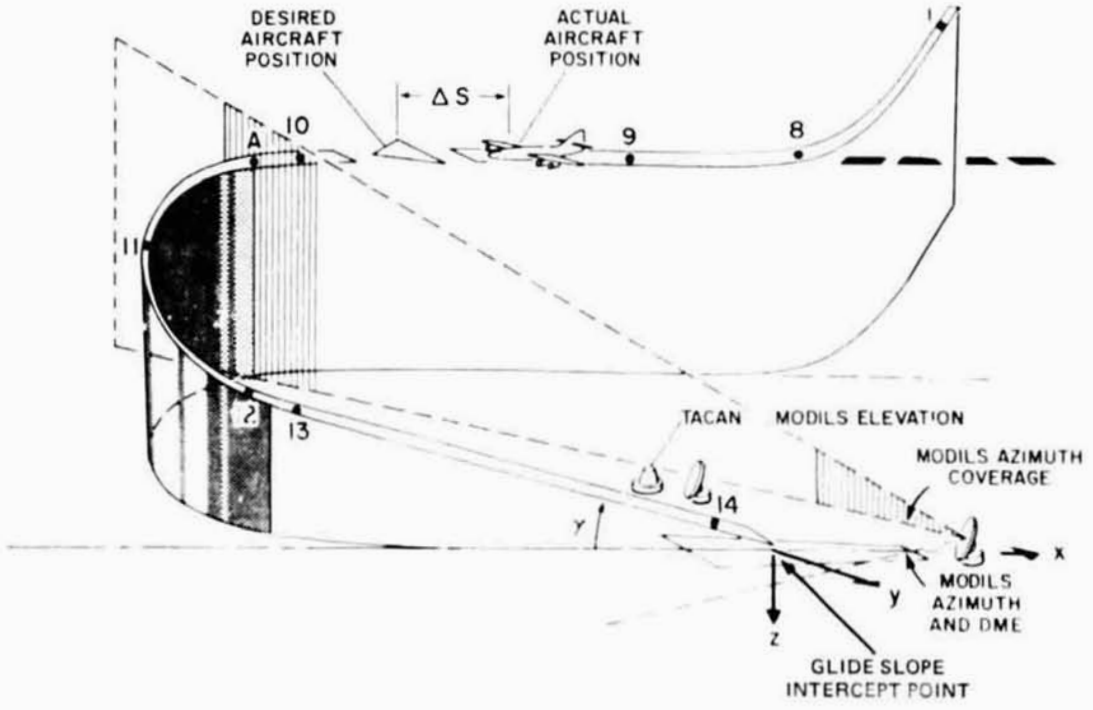

Figure 4.- Approach flightpath.

flightpath and to monitor the system. A detailed description of the operation of the system is given in reference 4.

The navigation system used provides estimates of the aircraft position and velocity with respect to a runway coordinate system which has its origin at the glide-slope intercept point (fig. 4). The position and velocity estimate are generated using ground navigation aid information blended in a complementary filter with inertial information obtained from body-mounted accelerometers and attitude sensors, and air data obtained from a barometric altimeter and an airspeed sensor. The ground navigation data are obtained from TACAN except when the aircraft is in MODILS coverage after passing point A (fig. 4). The navigation system also estimates wind velocity utilizing air data. In the event of a momentary loss of ground radio navigation aid information, navigation is accomplished by dead reckoning using air data. Upon regaining radio information, the system automatically switches back to the use of radio data. A detailed description of the navigation system is presented in reference 5.

The RNAV system used during the landing approach is based on a flightpath, stored in the airborne computer. The flightpath is specified by waypoints (X,Y,Z coordinates) and associated information such as the radius of turn between waypoints and the maximum, minimum, and nominal airspeed between waypoints. An illustration of an approach flightpath flown in the CV-340 is shown in figure 4. It consists of a long inbound leg (waypoints 1-10), a 180° turn to final approach with a 5° glide slope occurring halfway around the turn (waypoints 10-12), and a final straight-in approach (waypoints 12-14). A brief summary description of the 4D RNAV system is given next. A detailed description of the system is given in appendix A.

The approach guidance is initiated when the aircraft captures the rear extension of the straight line between waypoints (e.g., between waypoints 8 and 9; see dashed line, fig. 4). At waypoint 8, controlled time-of-arrival (4D) guidance is initiated. Slightly before waypoint 10, a predictive bank angle command is given, and just before waypoint 11, a constant vertical acceleration maneuver is performed to acquire the 5° flightpath angle. The short straight-in section (waypoints 12-13) is the last segment using the 4D guidance laws given below. The remaining flightpath to flare is flown with similar lateral and longitudinal guidance laws except for the system gains, which are relatively high from waypoint 13 to flare to assure precise path tracking.

For lateral tracking, the guidance law is:

$$\phi_c = K_1 Y_{err} + K_2 \dot{Y} + \phi_p \tag{1}$$

where ϕ_p equals zero, for a straight line track, and for a circular track,

$$\phi_p = \tan^{-1} \frac{V^2}{Rg} \tag{2}$$

For vertical tracking, the guidance law is:

$$\theta_c = \frac{K_3}{V_g} h_{err} + K_4 \gamma_{err} + \frac{K_5}{V_g} \int h_{err}\, dt \qquad (3)$$

As previously stated, 4D RNAV is initiated at waypoint 8 (fig. 4). From this point, the system attempts to arrive at waypoint 13 at a given time. Control of arrival time at waypoint 13 is based only on speed control, which is provided by controlling the throttle as a function of an airspeed error. In the flight director mode, the airspeed command is displayed on the EADI. The airspeed command V_{cref} is defined as the algebraic sum of a prescribed nominal airspeed (V_{AN}) and an error that is proportional to an aircraft position error (ΔS):

$$V_{cref} = V_{AN} - 0.04\Delta S \text{ (m/sec)} \qquad (4)$$

where ΔS is the distance along the track from the estimated aircraft position to a moving target, which represents the desired aircraft position (fig. 4). As the aircraft arrives at waypoint 8, the target and aircraft positions are made to coincide. The computed nominal arrival time at waypoint 13 is based on the time it would take to fly from waypoint 8 provided the aircraft flew the path exactly at the nominal airspeed and provided that there was no wind. To account for winds, the position of the moving target is recomputed every 10 sec based on the latest estimate of wind velocity and direction. This new computed target position assures that the target will arrive at waypoint 13 at the nominal arrival time while moving at the nominal airspeed. If the wind were changing during the approach, the computed positions of the target would have step changes every 10 sec which would result in excessive throttle activity. To limit the throttle activity, the time rate of change in the value of ΔS in the above equation is limited to 6.1 m/sec. For safety and other operational requirements, the airspeed command V_{cref} is limited to preset maximum and minimum airspeeds.

RESULTS AND DISCUSSION

As previously noted, the primary purpose of flight tests in the CV-340 was to validate the operation of the STOLAND system and to obtain preliminary insight into the performance of the navigation and guidance system. The data presented are from a set of 20 simulated IFR (hooded) approaches, which were flown at the Crows Landing Test Facility (shown in fig. 5 and described in detail in ref. 5). It includes a simulated STOL runway, which is 609.5 m long, a TACAN station for navigation, and an experimental microwave landing system (MODILS). It also includes a tracking radar to provide tracking data for independent postflight calculation of navigation errors. The tracking data were smoothed with a minimum mean square second-order curve fit over ±3 sec to obtain a best estimate of the actual aircraft position.

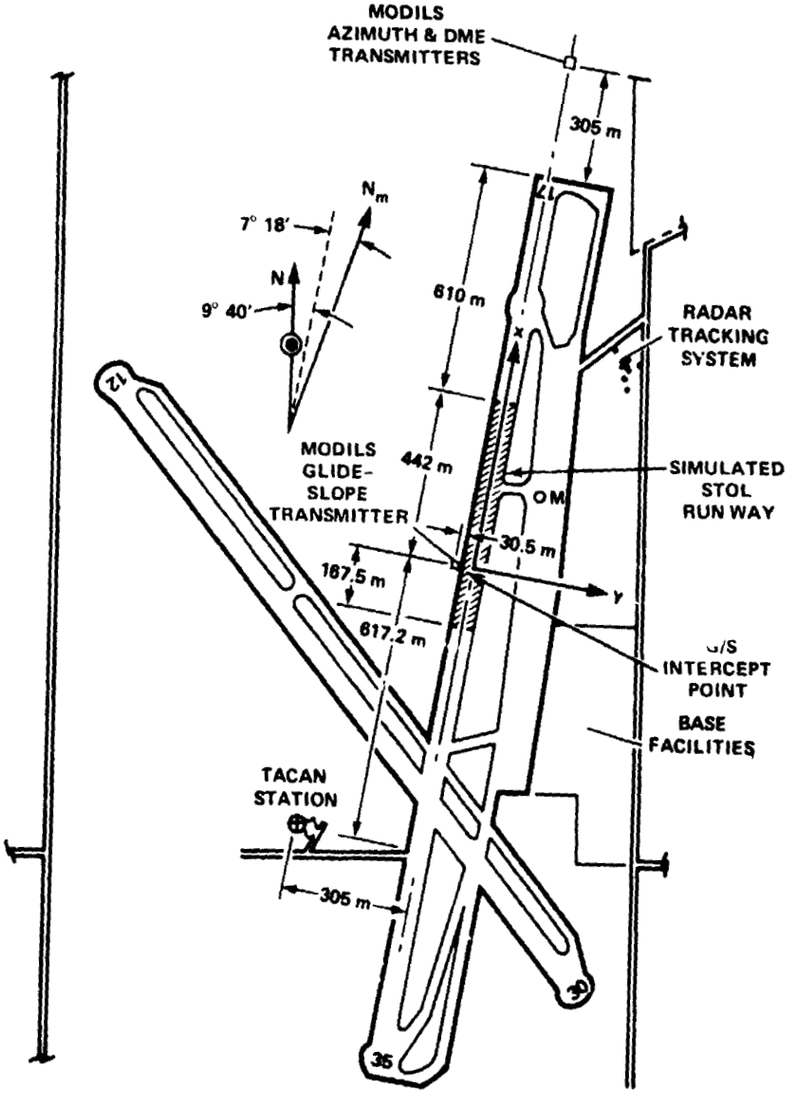

Figure 5.- Ground support equipment deployment at Crows Landing.

Representative performance of the guidance and navigation systems along a typical flightpath will be given.

Flightpath Description

Figure 6 shows orthographic projections of (1) the reference approach paths and associated waypoints, (2) the aircraft position as measured by radar for a typical flight test run, and (3) the position as computed by the onboard navigation system. Sixteen left and four right turning approaches were flown on two different days to study the effects of navigation aid bias errors on navigation and guidance.

The left and right turning flights are presented separately, since the errors resulting from the navigation aid bias errors depend on the flightpath. Figure 6(a) shows that the example left approach was initiated to the right and above the reference path. Up to and through the turn to the final approach, the aircraft remained to the right of the path and then acquired the runway centerline, maintaining that course for the remainder of the approach. During G/S tracking, the aircraft converged linearly from 30 m to 20 m above the reference path. This may be attributed to a MODILS elevation bias error of about 0.4°. The major error prior to MODILS acquisition can be attributed to the effect of the TACAN DME bias. Figure 6(b) shows similar results for a right turning approach.

Wind Environment

Following is a description of the x and y wind components which were encountered during the test flights, as estimated by the navigation system. For the first day, the x wind along the runway was a relatively steady tail wind of 7.3 m/sec. The y wind was -6 m/sec (from the left) at the 506-m approach altitude and reduced almost linearly to 0 m/sec at the altitude at which the approach was terminated (30 m). On the second day, the x wind component was a tail wind of 10 m/sec, and the y wind component linearly changed with decreasing altitude from -4.6 m/sec to 1.5 m/sec at the approach termination altitude.

Navigation and Guidance Errors

The navigation errors (shown in figs. 7, 9, and 11) include the ground navaid and airborne receiver signal errors, off nominal atmosphere effects on the altimeter, errors in the radar tracking data, and the basic navigation system errors resulting from software/hardware mechanization. The corresponding guidance errors are shown in figures 8, 10, and 12. In these figures, the abscissa is the distance (S) along the track. For orientation, the waypoints are labeled on the figures. Waypoints 10, 11, and 12 describe the final turn, and waypoint 13 is the final waypoint for 4D RNAV. Data are given for a typical flight along with the envelope of all data. The derivation of the equations for the navigation error calculations is given in appendix B. Navigation

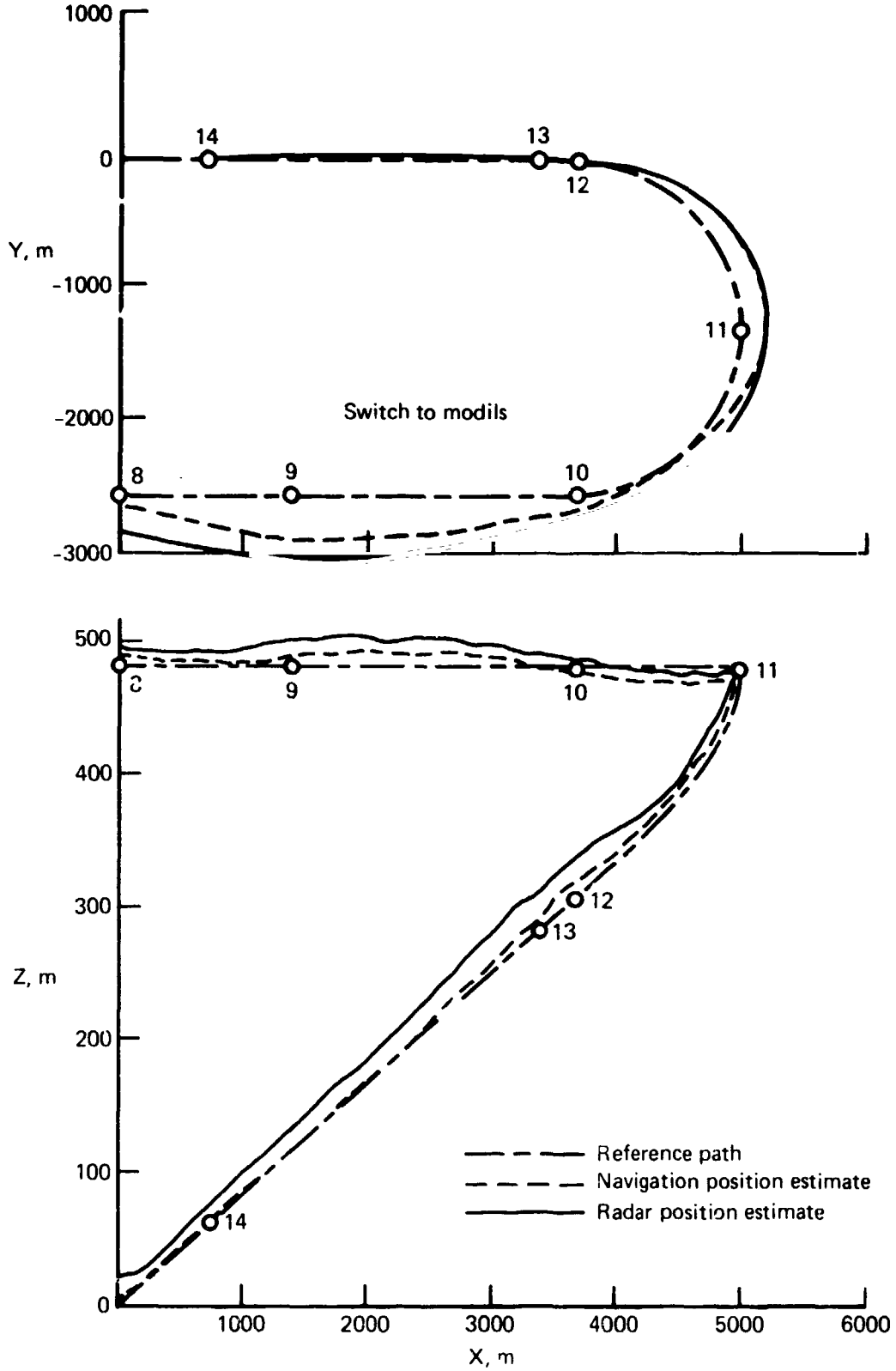

(a) Left turn.

Figure 6.- Approach flights.

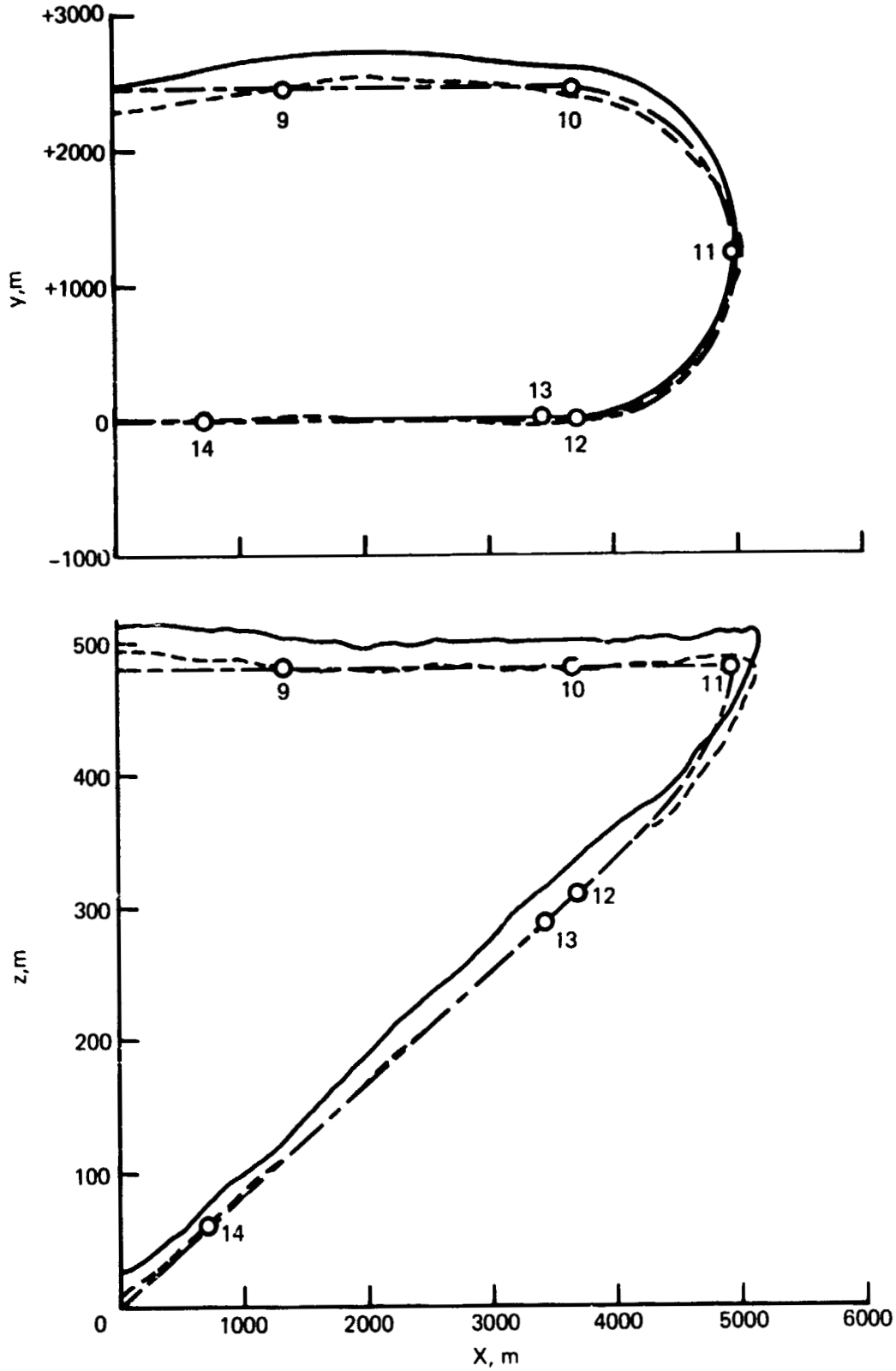

(b) Right turn.

Figure 6.- Concluded.

errors are positive if the estimated position along the flightpath is ahead or to the left of the actual (radar-derived) position. Guidance errors are positive if the estimated position is ahead or to the left of the reference position.

Crosstrack navigation errors- The crosstrack navigation error is the difference between the crosstrack positions as measured by the precision radar and the STOLAND navigation estimate. For the left-turning flightpaths of figure 6(a), the envelope of lateral navigation errors is shown in figure 7(a). At the initiation of the approach at waypoint 8, errors as large as 200 m occur. These errors converge to less than 70 m at the initiation of the turn at waypoint 10, where they start to increase again to values as large as 150 m. Examination of the data indicate that these navigation errors result from TACAN bias errors in both range and azimuth. A short time after passing waypoint 10, the transition from TACAN to MODILS navigation is initiated. Navigation errors then converge smoothly to less than 15 m after transition to MODILS is completed.

For the right-turning flightpaths of figure 6(b), the navigation errors show a different, but equally consistent, pattern (fig. 7(b)). Here, the TACAN DME error causes the aircraft to be flown on the left side of the nominal reference path. The errors after transition from TACAN to MODILS are eventually reduced to values similar to those shown in figure 7(a), since the flightpaths are common from waypoint 12 on. It will be noted that the envelope of figure 7(b) is narrower than that of figure 7(a). This is simply because the 4 right-turning flights were conducted on one day, whereas 16 left-turning flights were conducted on two different days; experience has shown that the navaids have different bias errors on different days. In contrast, a comparison of the data for the four left and four right approaches on the same day showed that they both had narrow envelopes.

Crosstrack guidance errors- The error shown in figure 8(a) is the difference between the onboard estimate of position and the minimum distance to the reference flightpath. The envelope of the crosstrack guidance error shows large errors at the initiation of the approach due to the use of different capture maneuvers. As a result of guidance activity, these errors converge to smaller values before switching to MODILS. To explain what happens between waypoints 10 and 11, one must consider the effect of transitioning between navaids with different bias errors. After switching to the more accurate navigation aid shortly after waypoint 10, the new position estimate rather quickly indicates that the aircraft is not on the reference path but to the right of it. This accounts for the sudden increase in guidance error, for which the pilot has to correct. The low-gain 4D RNAV lateral guidance law slowly guides the aircraft back to the reference path until, after passing waypoint 11, the guidance errors converge to small values. Finally, the high-gain localizer tracking law, which takes over after waypoint 13, converges the guidance errors to a narrow range of ±20 m when the aircraft is 1600 m from touchdown. Figure 8(b) shows a trend similar to figure 8(a). Positive guidance errors in this case mean that the onboard navigation system estimates that the aircraft is slightly on the left of the reference path.

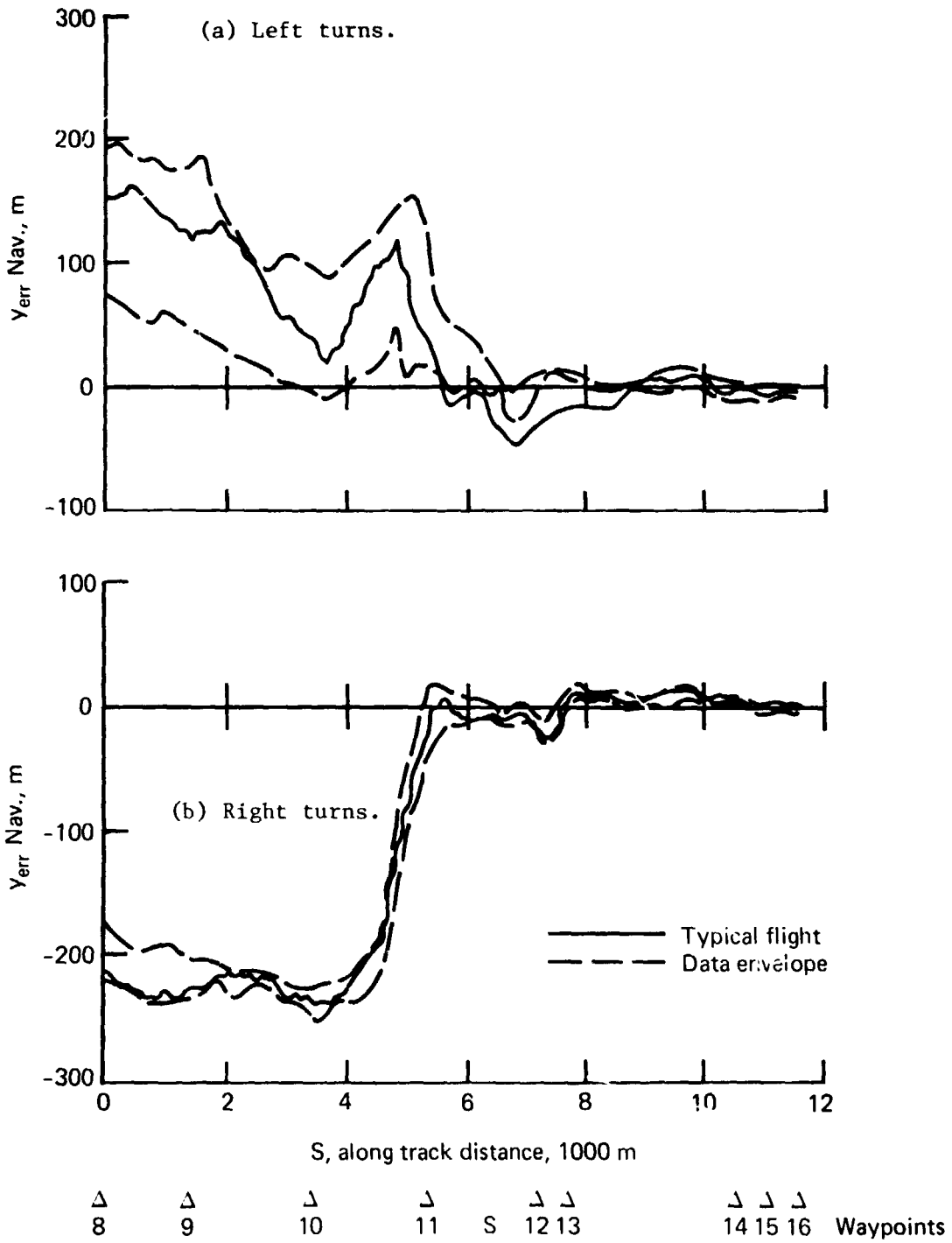

Figure 7.- Crosstrack navigation errors.

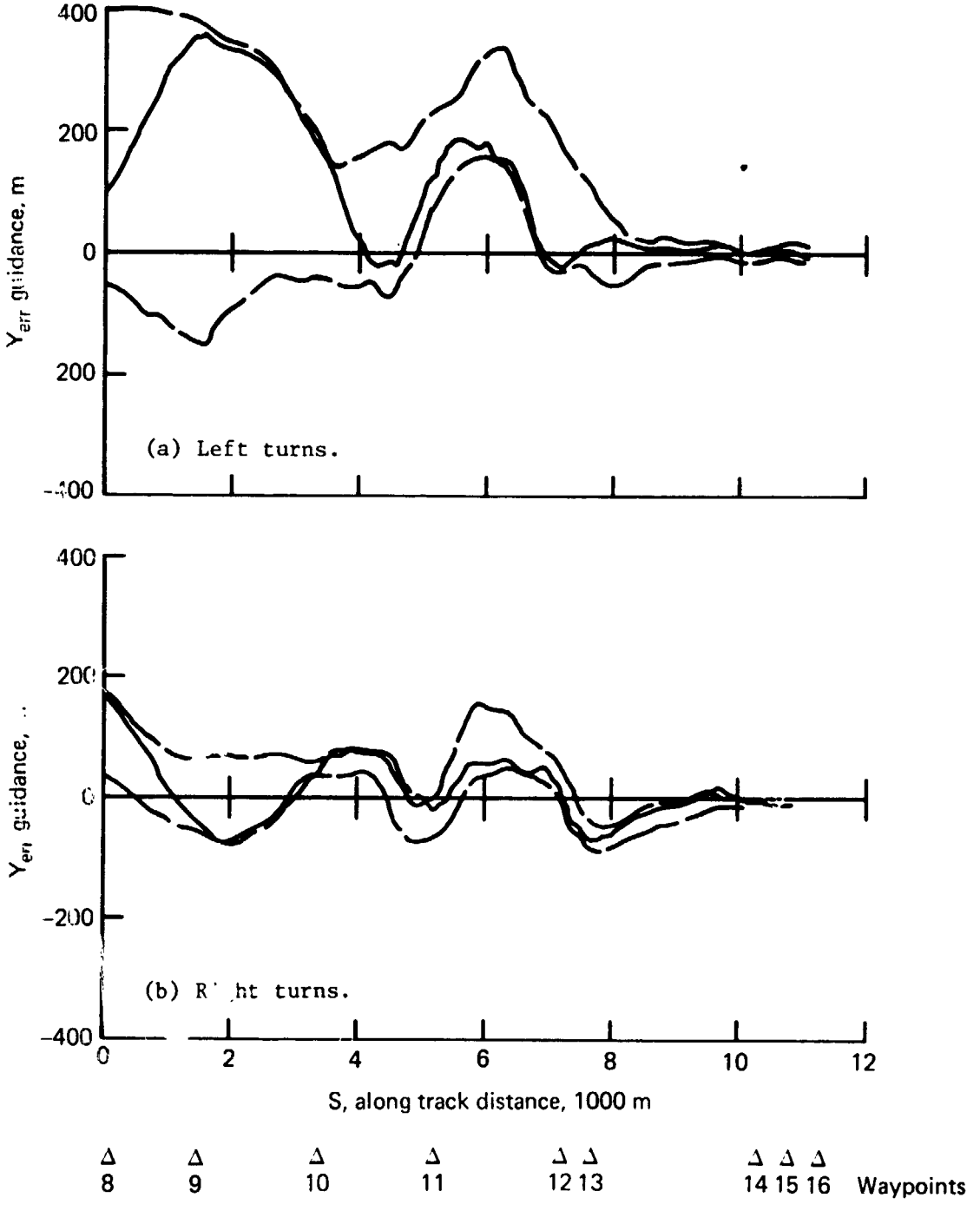

Figure 8.- Crosstrack guidance errors.

Vertical navigation errors- The envelope of the vertical navigation errors, figure 9(a), shows errors as large as 24 m at initiation of the approach. The vertical navigation errors are always positive and are probably the result of a bias in the baro-altimeter. It should be noted that the baro-altimeter reference was set before each approach, based on information radioed from the control tower. This setting only assures that the barometric altitude coincides with the geometric altitude at the runway level. As a result, different bias errors occurred on each approach, which makes the envelope in figure 9(a) fairly wide. After transition to MODILS and the start of the descent at waypoint 11, the baro-altimeter measurement is slowly combined with, and, after 1 min, fully replaced by the MODILS data, to prevent a step change in estimated altitude at the initiation of glide-slope tracking. Due to a constant 0.4° MODILS elevation bias error,[1] the vertical navigation error past waypoint 13 converges linearly with distance from the MODILS elevation antenna. After waypoint 13, the width of the error envelope is approximately 8 m. Figure 9(b) illustrates the same sequence of events for right turns: (1) there was an initial barometric bias error of about 10 m past waypoint 10, (2) during the 1-min transition to MODILS data, the errors increased due to the MODILS elevation bias error, and (3) for the straight-in tracking past waypoint 13, the errors decreased linearly as before. A comparison of the data for the four left and four right approaches on the same day showed that the barometric altitudes had the same bias errors.

Vertical guidance errors- The envelope of vertical guidance errors (fig. 10(a)) shows a range of errors as large as 15 m at the initiation of the approach at waypoint 8 and is generally above the desired path. The magnitude of the error represented by the envelope width remains approximately constant between waypoints 8 and 10. The vertical guidance error in figure 10 is blanked out during the -5.0° flightpath angle capture maneuver, which starts approximately at waypoint 11. The vertical guidance error during this maneuver has no meaning since the capture law between path segments does not use the altitude error, but it is a closed loop law based on a linearly varying flightpath angle command, $\theta_c = K(\gamma - \gamma_{ref})$.[2] Between waypoints 13 and 14, the vertical guidance error envelope converges to about ±3 m as a result of the high-gain guidance law and high-gain navigation filters used during the final straight-in approach. The guidance errors in figure 10(b) are very similar to those in figure 10(a), although the character is somewhat different since the corresponding navigation errors have different spatial changes.

Alongtrack navigation errors- The alongtrack navigation errors, shown in figure 11, contribute to time-of-arrival errors at the final waypoint. As expected, the navigation errors have different characteristics for left and right approaches, since the bias errors distort the measured flightpaths differently. The error trend is even different in the early common portion of the flightpath (past waypoint 13), although the MODILS azimuth bias errors

---

[1]In later flights, the MODILS elevation bias error was reduced considerably.

[2]In an advanced version of this system, the capture law was replaced by guidance along a circular arc as in equation (3) where h_{err} is the deviation from the arc.

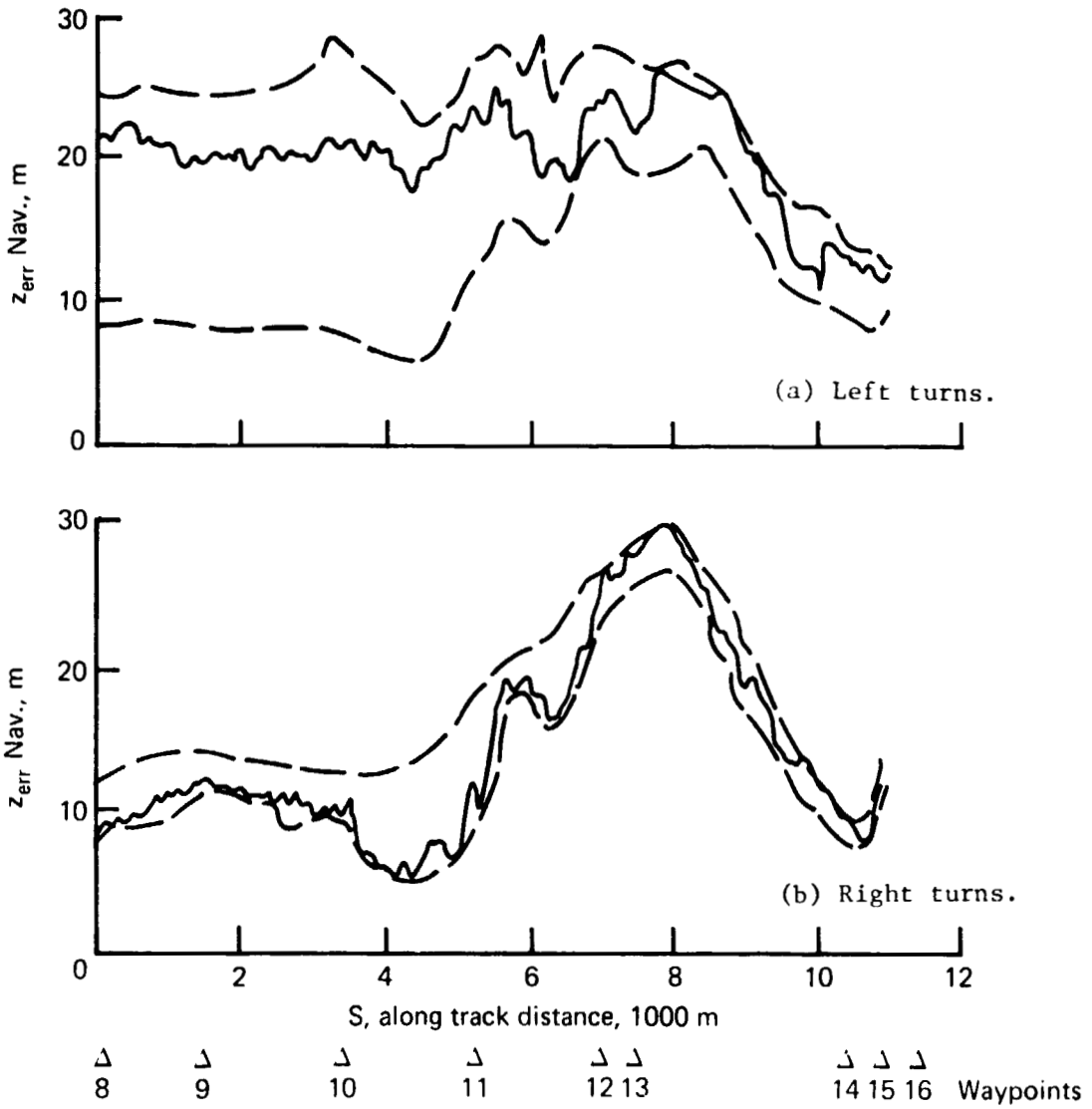

Figure 9.- Vertical navigation errors.

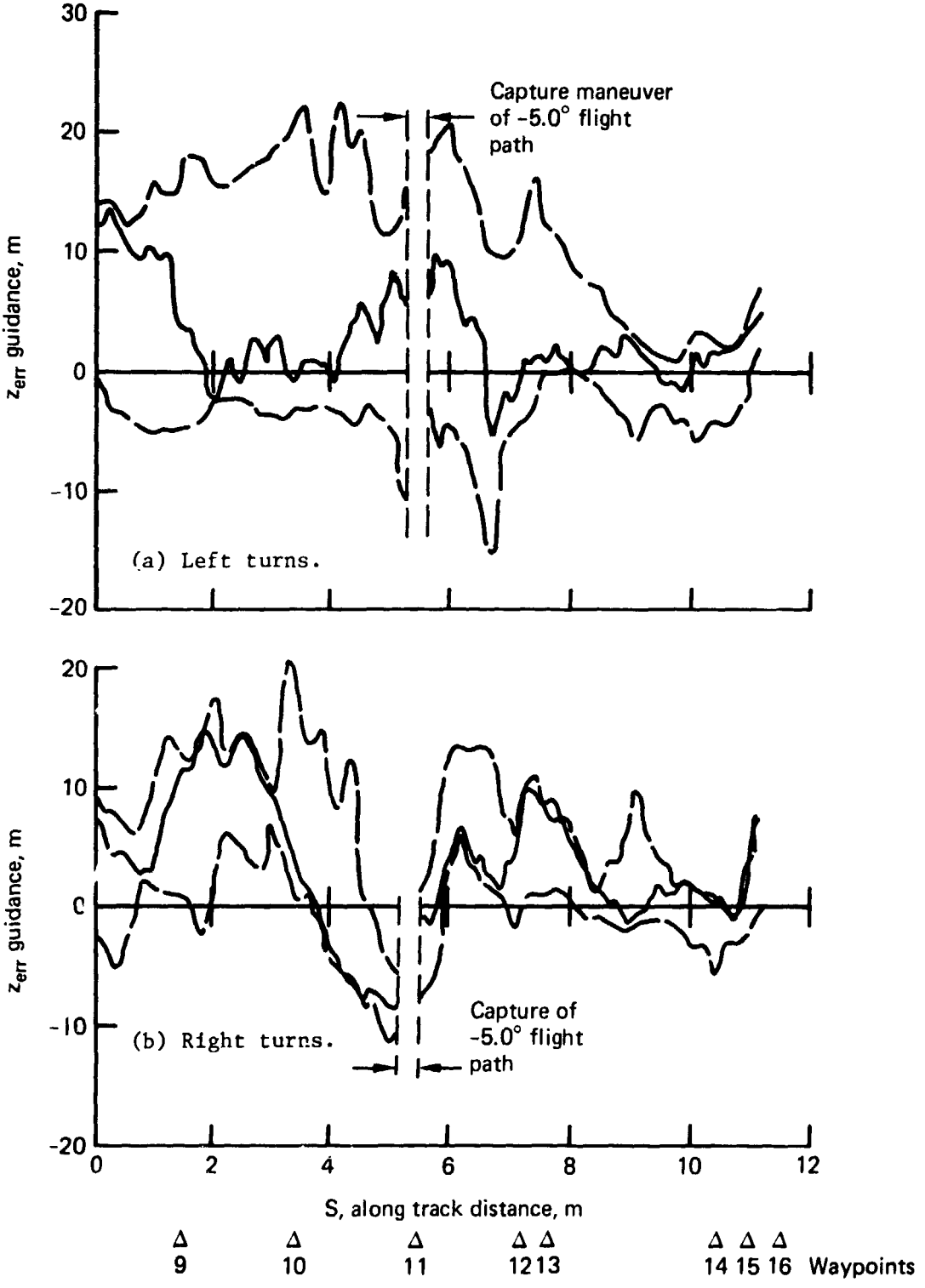

Figure 10.- Vertical guidance errors.

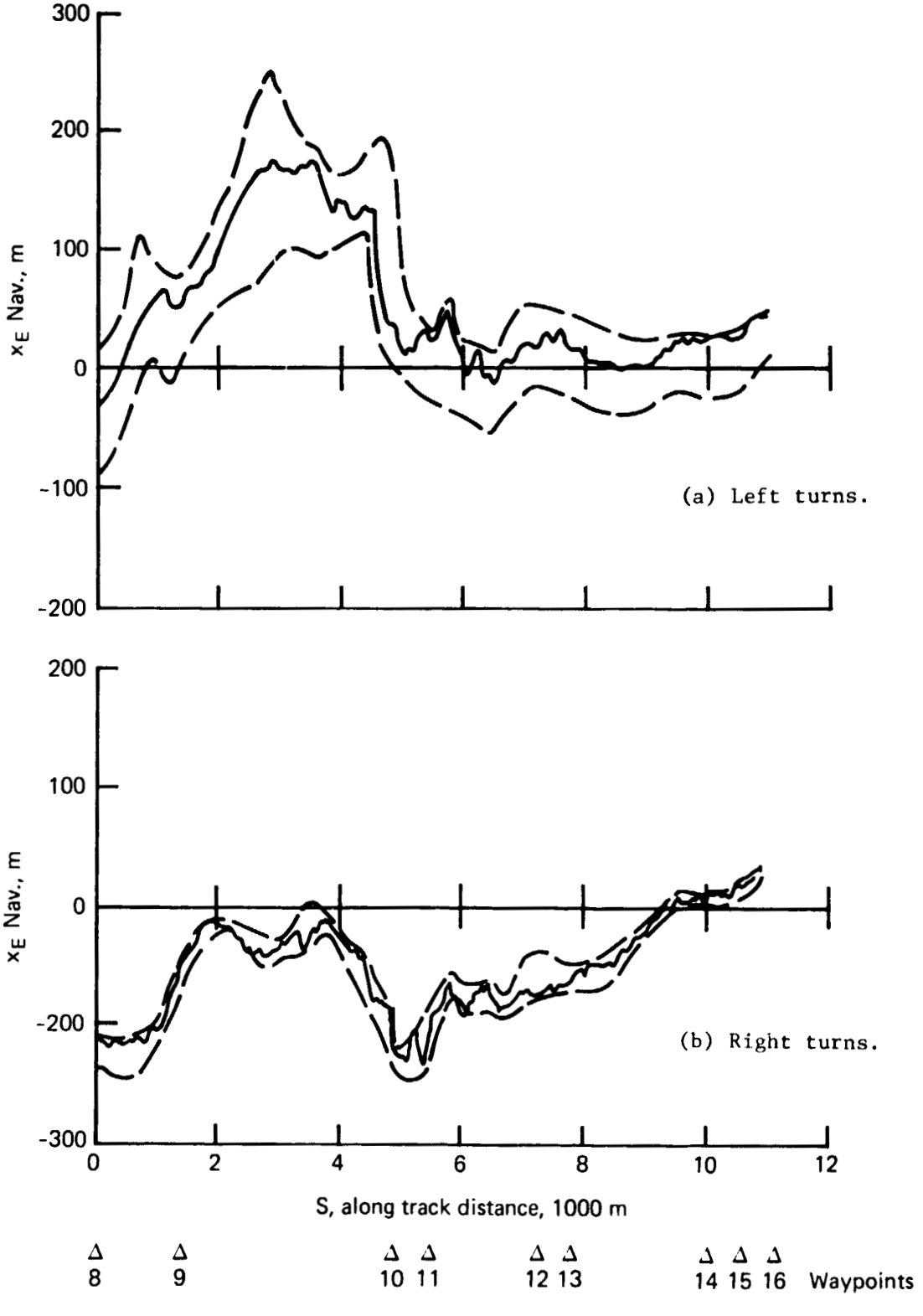

Figure 11.- Alongtrack navigation errors.

did not change. The difference is explained by the long time constant of the X-navigation filter, and the fact that the filter had different bias error inputs before reaching waypoint 13.

Alongtrack guidance errors- Typical alongtrack guidance errors are shown in figure 12 for left and right turns. These were used to command airspeed corrections on the EADI based on the control law $V_c = V_n + 0.04\Delta S_L$. Again, the characteristics of the curves are different for left and right turns, and similar for turns in the same direction. However, the dependence of the guidance errors on the navigation errors and the pilot control was not analyzed in detail, because (1) some of the wind calculations for turns, which were used for nominal time-of-arrival calculations, were later found to be in error (see eqs. (A41) and (A42) in appendix A); (2) only the rate-limited $\Delta S, (\Delta S_L)$, has been recorded, and (3) the throttle position, which is the pilot response to the indicated error, was not recorded.

Comparison of figures 12(a) and 12(b) shows that the average time error at the final waypoint (expressed as ΔS_L errors) is smaller for the right turns than for the left turns. A reason for this can be seen from figures 6(a) and 6(b), which are typical of all approaches. The left turning flightpath (fig. 6(a)) is several hundred meters longer than the reference flightpath. This difference must be made up by speed control, but the final waypoint (13) is too close for a complete correction due to the limited speed variations available. In contrast, for the right-turning flightpaths, the aircraft flew a shorter path on the inside of the reference path, and, therefore, it did not have to make up for increased path length with speed control.

Time-of-Arrival Errors at Waypoint 13

Figure 13 is a histogram of the time-of-arrival errors at waypoint 13 for the simulated instrument (hooded) approaches. For these tests, the mean time-of-arrival error is 3.1 sec (late) with 2σ deviation of ±4.3 sec. The mean time-of-arrival error obtained during these tests may result from the TACAN range error which caused the actual longitudinal distance flown to be longer than the reference path. Additional data are required to establish the system performance for all TACAN and MODILS error combinations.

It is interesting to note that current manual guidance techniques enable air traffic controllers to deliver CTOL aircraft to the runway within about ±15 sec of the predicted arrival time (ref. 10). This capability corresponds to a single runway acceptance rate of about 40 IFR arrivals per hour using current separation standards. Using the improved capability of the automatic time-of-arrival guidance system described here, it would be possible to increase the runway acceptance rate by about 40 percent (see ref. 10).

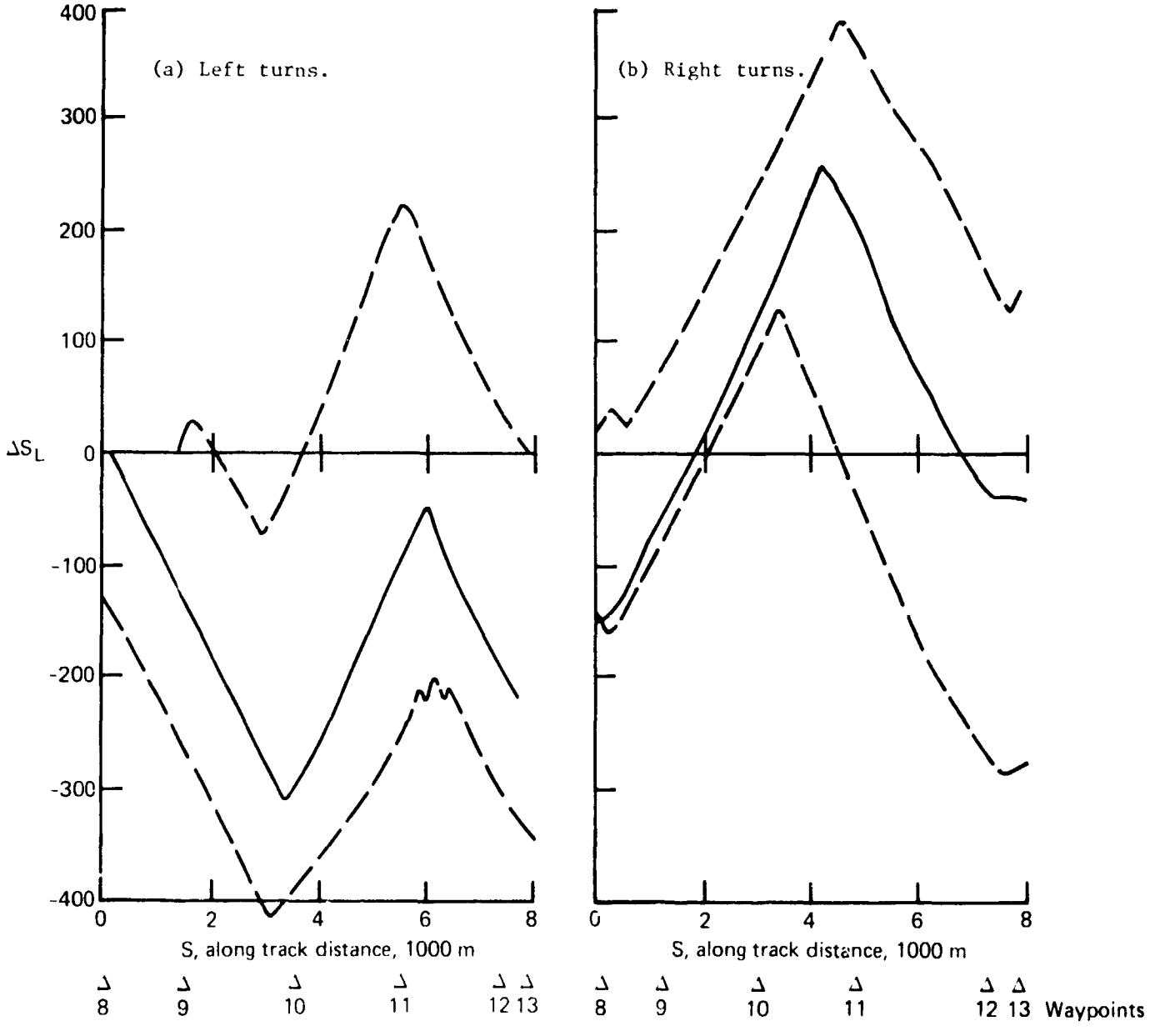

Figure 12.- Alongtrack guidance errors.

Figure 13.- Approach flights.

CONCLUSIONS

Results are presented for 20 flight director approaches made during an investigation of a 4D RNAV system using the NASA CV-340 aircraft. Results of these limited tests led to the following conclusions:

1. Blended radio/inertial navigation using TACAN and a microwave scanning beam landing guidance system (MODILS) permitted a smooth transition from area navigation (TACAN) to precision terminal navigation (MODILS).

2. Time of arrival at a point about 2 n. mi. (3.70 km) from touchdown was about 3 sec ±4 sec (2σ) later than the computed nominal arrival time.

3. Navigation system bias errors (rather than system noise) are primarily responsible for the distortion of the flightpaths and the character of the guidance errors.

APPENDIX A

STOLAND 4D RNAV

INTRODUCTION

The purpose of this appendix is to give a technical overview description of the STOLAND 4D RNAV system which was used to obtain the experimental data in this report. The experimental tests had limited objectives, and the system was designed with these objectives in mind. The primary purpose was to test path guidance concepts, including time-of-arrival control, once the reference path was acquired. The system was designed primarily for automatic guidance. However, for the tests described in the body of the report, flight director commands were obtained through further processing of the guidance system commands. For completeness, this processing will also be described in the appendix.

The navigation system, which computes estimates of position $\hat{x}$, $\hat{y}$, $\hat{z}$, ground speeds $\dot{\hat{x}}$, $\dot{\hat{y}}$, $\dot{\hat{z}}$, and wind components $\hat{\dot{x}}_w$, $\hat{\dot{y}}_w$ in a runway coordinate system, has been described elsewhere (ref. 6). In this appendix, equations will be given that transform the navigation quantities into values relative to the flightpath, as needed in the guidance computations.

FLIGHTPATH DESIGN CONSIDERATIONS

The reference flightpath must be capable of being flown under all environmental conditions, particularly wind and turbulence, given the aircraft performance limitations and control authority limits. In order to limit the complexity of in-flight computations, a few requirements are made on the geometry of the trajectory and on the location of the waypoints.

Segments between waypoints must be either completely linear or completely circular. Circular flightpath segments must have large enough radii so that the roll angle command will not exceed some specified limit, say 30°, for wind conditions likely to be encountered with the maximum specified airspeed (for time-of-arrival control), allowing a margin for path error correction.

Straight-line and circular flightpath sections must be connected in such a manner that the circles are tangent to the straight lines. The first circular segment must be entered from a straight line segment. After the first segment, there is no restriction on the number of subsequent circular segments that may be contiguous except that there must be no discontinuities in direction of the trajectory between a circular segment and any contiguous segment. Segments between waypoints must represent flightpaths that the aircraft can fly within the specified airspeeds. Straight-line flightpath

segments may follow each other without a connecting circular segment. In this case, the system will perform appropriate capture maneuvers between line segments. In the present STOLAND configuration, the final line segment of the 4D RNAV flightpath must be an extension of the glide slope and localizer tra to be flown to touchdown. The prescribed airspeed and airspeed limits vary linearly between the reference values defined at the waypoints.

Flightpath Definition

Parameters that define the flightpath- In STOLAND, provision is made for four prestored flightpaths, each defined by a maximum of 30 waypoints. Each waypoint is specified by seven quantities (x, y, z, R, V_{max}, V_{min}, and V_{ref}). The x, y, and z are coordinates of the waypoint with respect to a terminal area (runway oriente) coordinate frame. The radius of curvature R is specified when a specific flightpath curvature is desired. The polarity of R determines the direction of the turn, positive for right turn and negative for left turn. The waypoint at which R is specified represents the start of that specific curved path. If zero curvature is desired ($R = \infty$), then the notation used to recognize that a straight-line segment is desired is to enter zero in the R column. The terms V_{max}, V_{min}, and V_{ref} specify the maximum and minimum speeds allowable and the reference speed at the waypoints.

Auxiliary parameters- The information entered in the computer defines the flightpath, but it is insufficient to actually fly it and to display the flightpath on the multifunction display. For these purposes, information from two sequential waypoints is used to calculate auxiliary quantities, namely, the glide-slope angles, heading, and direction sine and cosine for straight-line sections, and the coordinates of the center of turn, heading change angle in the turn, and other quantities for circular line sections.

The auxiliary parameters used for the 3D and 4D RNAV are computed in an initialization routine following waypoint entry, after one of the four flightpaths is selected for display. If waypoints are changed in flight or on the ground, a reinitialization is performed.

The following parameters are computed for straight-line segments (fig. A1). The distance d_n is the distance along the specified flightpath between waypoints m and n:

$$d_n = \sqrt{(x_n - x_m)^2 + (y_n - y_m)^2} \tag{A1}$$

The next three parameters are constants that are related to the orientation of a line segment. The course is

$$\psi_{C_n} = \tan^{-1}\left(\frac{y_n - y_m}{x_n - x_m}\right) \tag{A2}$$

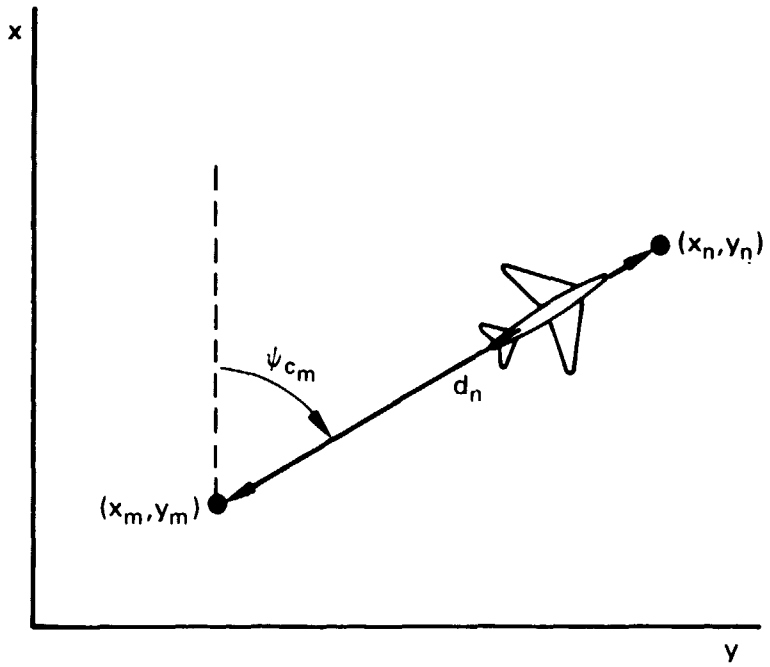

Figure A1.- Line segment.

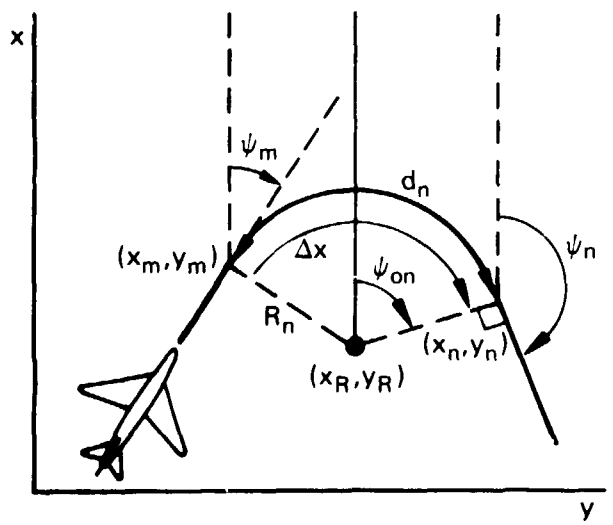

(a) Right turn.

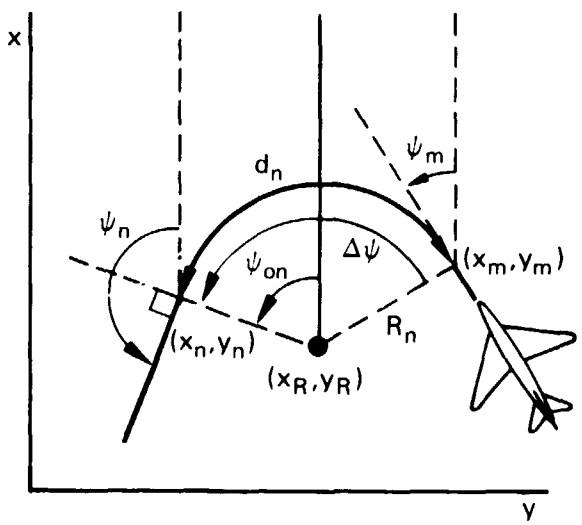

(b) Left turn.

Note: Angles shown to the right are positive; angles shown to the left are negative.

Figure A2.- Curved segment.

Direction sine and cosine are

$$a_n = \frac{y_n - y_m}{d_n} = \sin \psi_{C_n} \tag{A3}$$

$$b_n = \frac{x_n - x_m}{d_n} = \cos \psi_{C_n} \tag{A4}$$

The following parameters are computed for curved segments (fig. A2). Coordinates of the center of a circular segment are obtained from R_n, the radius of segment n, x_m, y_m, the coordinates at the start of segment n, and ψ_m, the course at point (x_m, y_m). If R_n is entered positive for right turn and negative for left turn, the equations are

$$x_{R_n} = R_n \cos\left(\psi_m + \frac{\pi}{2}\right) + x_m \tag{A5}$$

$$y_{R_n} = R_n \sin\left(\psi_m + \frac{\pi}{2}\right) + y_m \tag{A6}$$

For circular flightpaths, the course at the end of the turn ψ_n, the angle of turn $\Delta\psi$, and the arc length d_n between waypoints are defined below.

$$\psi_n = \tan^{-1}\left(\frac{y_n - y_R}{x_n - x_R}\right) + \text{sign}\left(R_n\right)\frac{\pi}{2}\ , \quad -\pi < \psi_n \leq \pi \tag{A7}$$

For a right turn (R positive),

$$\left.\begin{aligned} \Delta\psi &= \psi_n - \psi_m \quad \text{if} \quad \psi_n - \psi_m \geq 0 \\ \Delta\psi &= \psi_n - \psi_m + 2\pi \quad \text{if} \quad \psi_m - \psi_m < 0 \end{aligned}\right\} \tag{A8a}$$

For a left turn (R negative),

$$\left.\begin{aligned} \Delta\psi &= \psi_n - \psi_m - 2\pi \quad \text{if} \quad \psi_n - \psi_m \geq 0 \\ \Delta\psi &= \psi_n - \psi_m \quad \text{if} \quad \psi_n - \psi_m < 0 \end{aligned}\right\} \tag{A8b}$$

$$d_n = \left|R_n \Delta\psi\right| \tag{A9}$$

The nominal flightpath angle for both turning and straight-line segments is

$$\gamma_{ref} = \tan^{-1}\left(\frac{z_n - z_m}{d_n}\right) \tag{A10}$$

Another auxiliary parameter is D_n, the velocity gradient. It is used to calculate the nominal speeds and speed boundaries between waypoints.

$$D_n = \frac{V_{ref_n} - V_{ref_m}}{d_n} \tag{A11}$$

Note that the acceleration, dv/dt, is not constant in this case. Similar expressions hold between the minimum and maximum speed boundaries.

3D Flightpath Guidance Computations

The object of the flightpath guidance is to fly closely to the reference path, in spite of navigation errors and physical disturbances, without excessive control activity. Figure A3 shows the final portion of a typical flightpath used in the flight tests. It defines the guidance error quantities. It ends with a 180° turn onto the final leg. The last 90° of this final turn descends at a glide-slope angle of 5°. The final waypoint is about 1 min from touchdown.

Independent of path geometry, the path tracking guidance laws remain essentially the same, except for the reference quantities of flightpath angle γ_{ref} and nominal roll angle ϕ_p and some gains.

For lateral tracking, the guidance law uses the crosstrack error y_{err} to null the error and the crosstrack velocity $\dot{y}_{err}$ for lateral flightpath damping:

$$\phi_c = K_1 \dot{y}_{err} + K_2 y_{err} + \phi_p \tag{A12}$$

where the predicted roll angle is

$$\phi_p = 0 \tag{A13}$$

for a straight-line track, and

$$\phi_p = \tan^{-1}\left(\frac{V_g^2}{R_g}\right) \tag{A14}$$

for a circular track, where the ground speed is calculated from navigation data

$$V_g = \sqrt{\hat{\dot{x}}^2 + \hat{\dot{y}}^2} \tag{A15}$$

and $g = 10\ m/sec^2$.

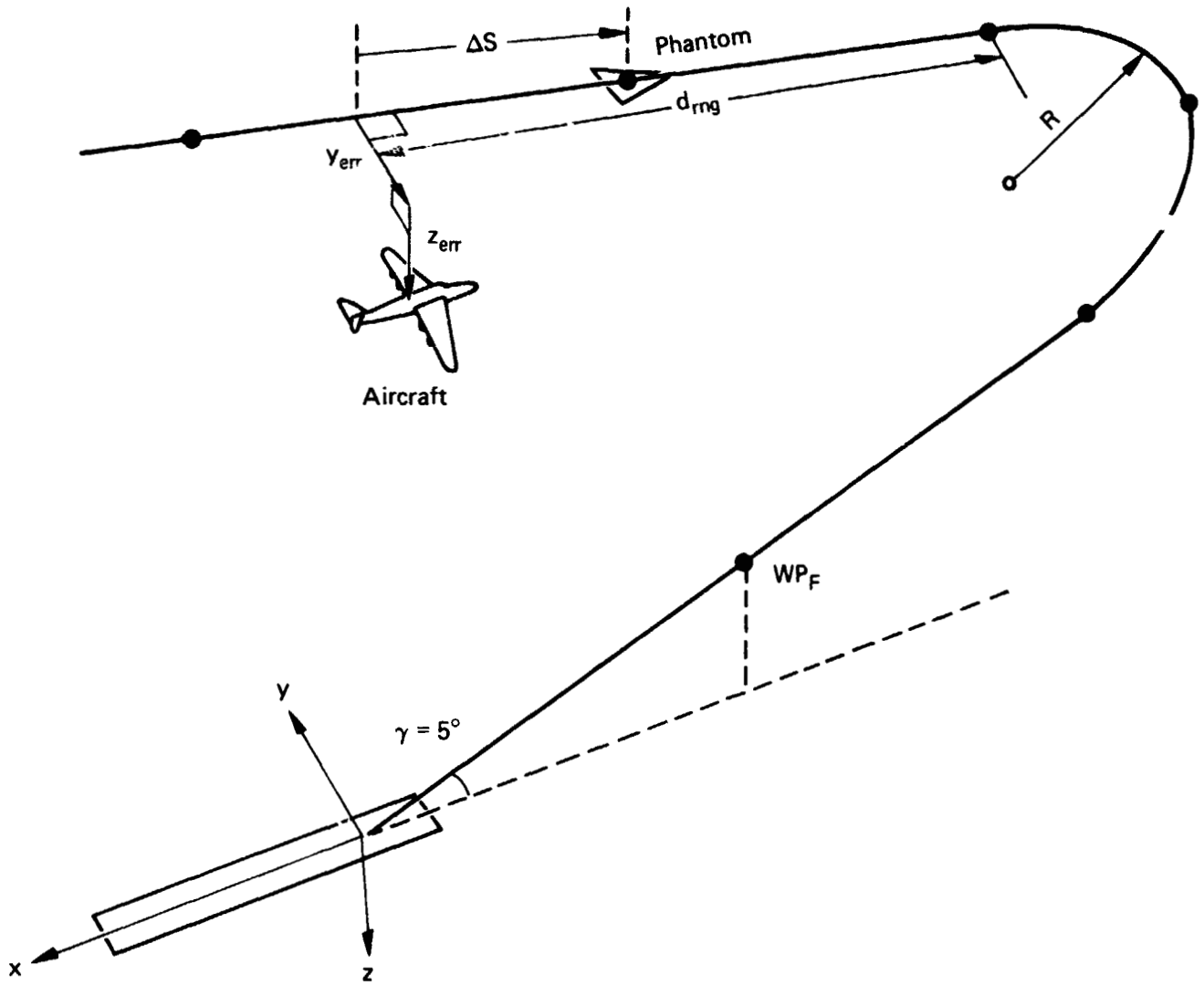

Figure A3.- 4D RNAV.

For vertical control, the pitch guidance law uses the altitude error z_{err} to null the error and the inertial flightpath angle error γ_{err} for vertical flightpath damping is

$$\theta_c = \frac{K_3}{V_g} z_{err} + K_4 \gamma_{err} + \frac{K_5}{V_g} \int z_{err} \tag{A16}$$

where the flightpath angle error is

$$\gamma_{err} = \gamma_{ref_n} - \gamma_I \tag{A17}$$

The inertial flightpath angle γ_I is calculated from navigation data. For small angles,

$$\gamma_I = \frac{\hat{\dot{z}}}{V_g} \tag{A18}$$

The remaining error quantities in the above guidance equations, y_{err}, $\dot{y}_{err}$, and z_{err}, are computed from flightpath and navigation data as follows. The aircraft path errors y_{err} and z_{err} are computed as horizontal and vertical distances from the flightpath as defined by a plane perpendicular to the flightpath which contains the center of gravity of the airplane. For a straight-line reference flightpath, the lateral deviation is (fig. A4)

$$y_{err} = a_n(\hat{x} - x_n) - b_n(\hat{y} - y_n) \tag{A19}$$

which is positive when the aircraft is on the left of the reference flightpath.

The crosstrack velocity is calculated from the navigation system ground speed estimates $\hat{\dot{x}}$ and $\hat{\dot{y}}$. For a straight-line path

$$\dot{y}_{err} = a_n \hat{\dot{x}} - b_n \hat{\dot{y}} \tag{A20}$$

From figure A5, the lateral deviation from a circular flightpath is

$$y_{err} = \text{sign}(R) \left[\sqrt{(x_R - \hat{x})^2 + (y_R - \hat{y})^2} - |R| \right] \tag{A21}$$

defined so that, in agreement with the straight-line flightpath, the error is positive if the aircraft is on the left of the flightpath for either right or left turns. The crosstrack speed error for a circular path is

$$\dot{y}_{err} = \text{sign}(R) \frac{(x_R - \hat{x})\hat{\dot{x}} + (y_R - \hat{y})\hat{\dot{y}}}{\sqrt{(x_R - \hat{x})^2 + (y_R - \hat{y})^2}} \tag{A22}$$

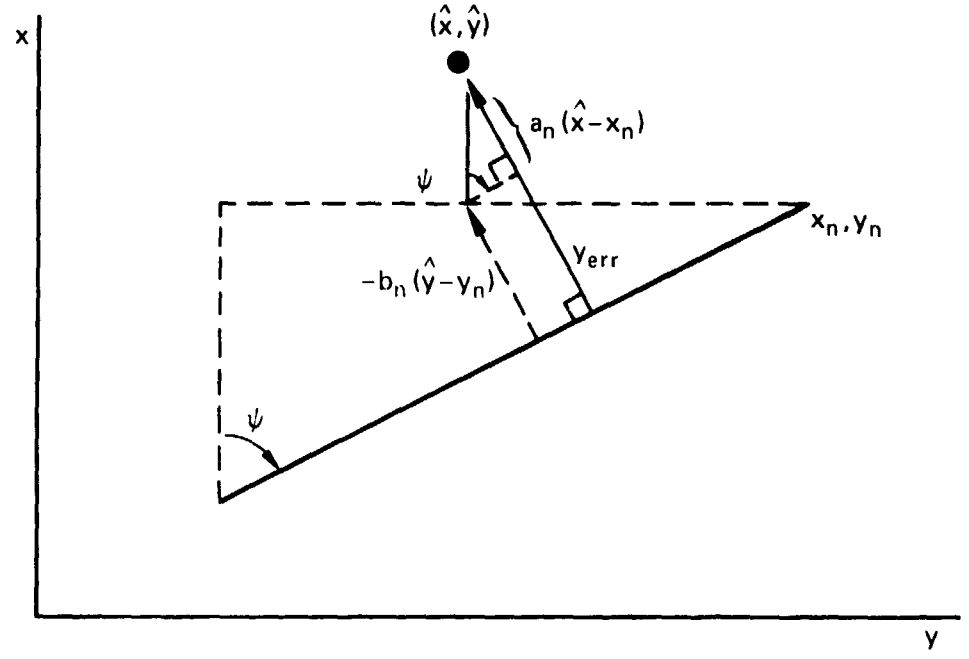

Figure A4.- Lateral deviation geometry for straight flightpath.

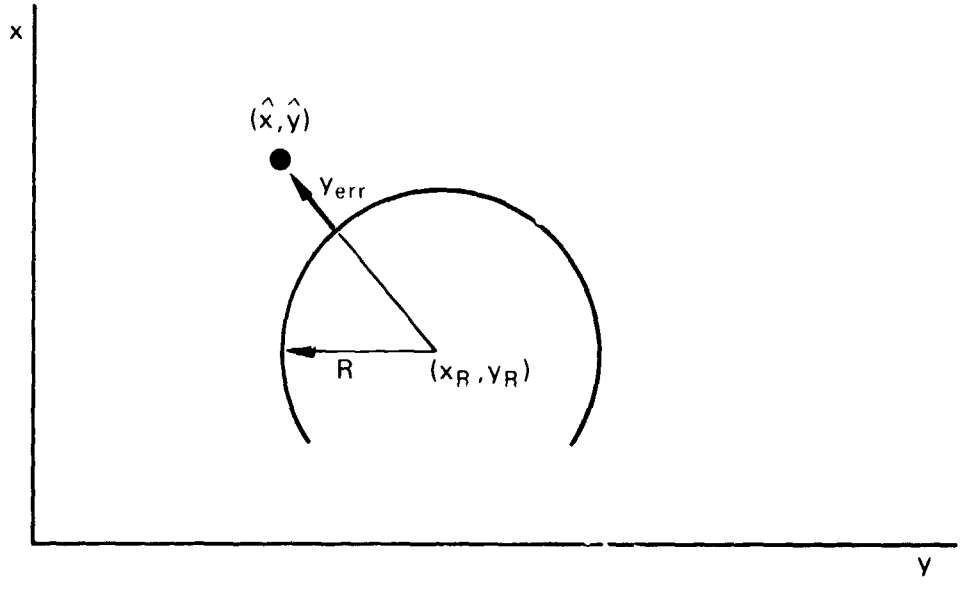

Figure A5.- Lateral deviation geometry for circular flightpath.

The vertical deviation from the reference flightpath is (fig. A6)

$$Z_{err} = (z_n - z_m) \frac{d_{rng}}{d_n} - z_n + \hat{z} \tag{A23}$$

Both straight and circular flightpaths require d_{rng}, the range to the next waypoint, for this error calculation. For a straight-line flightpath segment, the range to the next waypoint is

$$d_{rng} = \frac{x_n - \hat{x}}{b_n} \qquad b_n > a_n \tag{A24}$$

or

$$d_{rng} = \frac{y_n - \hat{y}}{a_n} \qquad a_n > b_n \tag{A25}$$

provided that the aircraft is close to the flightpath. That these are reasonable approximations for small crosstrack errors can be seen from the exact expressions which include the crosstrack distance y_{err} (fig. A7)

$$d_{rng} = \frac{x_n - \hat{x} + y_{err} \sin \psi_n}{\cos \psi_n} \tag{A26}$$

$$d_{rng} = \frac{y_n - \hat{y} - y_{err} \cos \psi_n}{\sin \psi_n} \tag{A27}$$

For a circular flightpath, the range from the aircraft to the next waypoint is (fig. A8)

$$d_{rng} = |R\Delta\psi| \tag{A28}$$

The complete calculations of equation (A28) are equivalent to those of equations (A7) to (A9) except that x_n and y_n are replaced by $\hat{x}$ and $\hat{y}$, and ψ_n is replaced by ψ_{ac}.

Path Segment Capture

Since the aircraft responds at a finite rate, and since passenger comfort must be observed, transition maneuvers are required between flightpath segments. Guidance law switching is accomplished by monitoring the distance d_{rng}. Before entering the next path segment, a capture maneuver is performed which will result in a smooth entry to that segment. This is important when the flightpath angle or turn radius is changed, and when transitioning between straight-line segments of different courses.

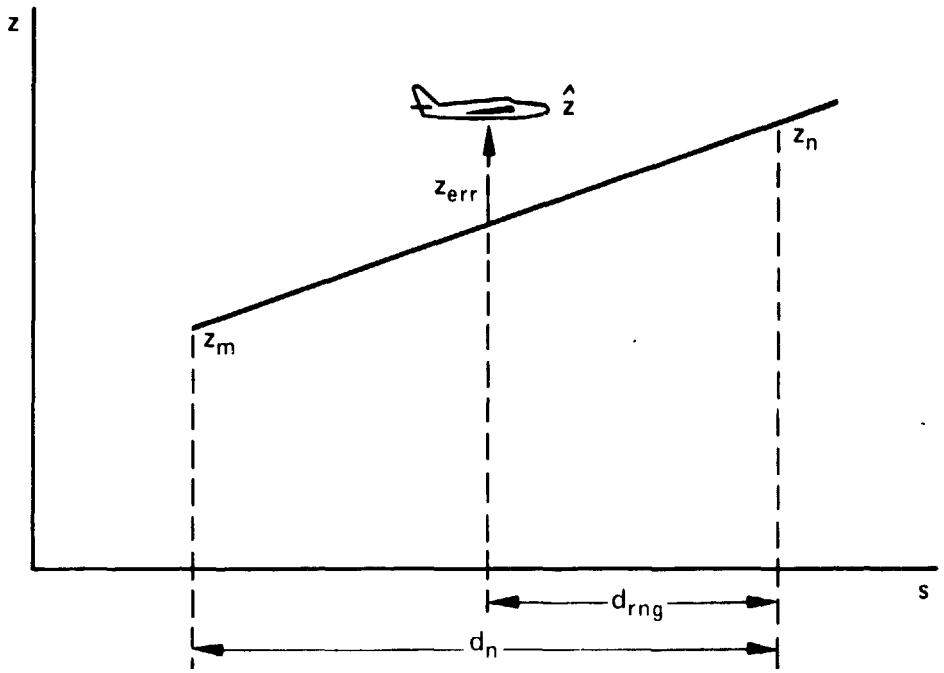

Figure A6.- Vertical deviation geometry.

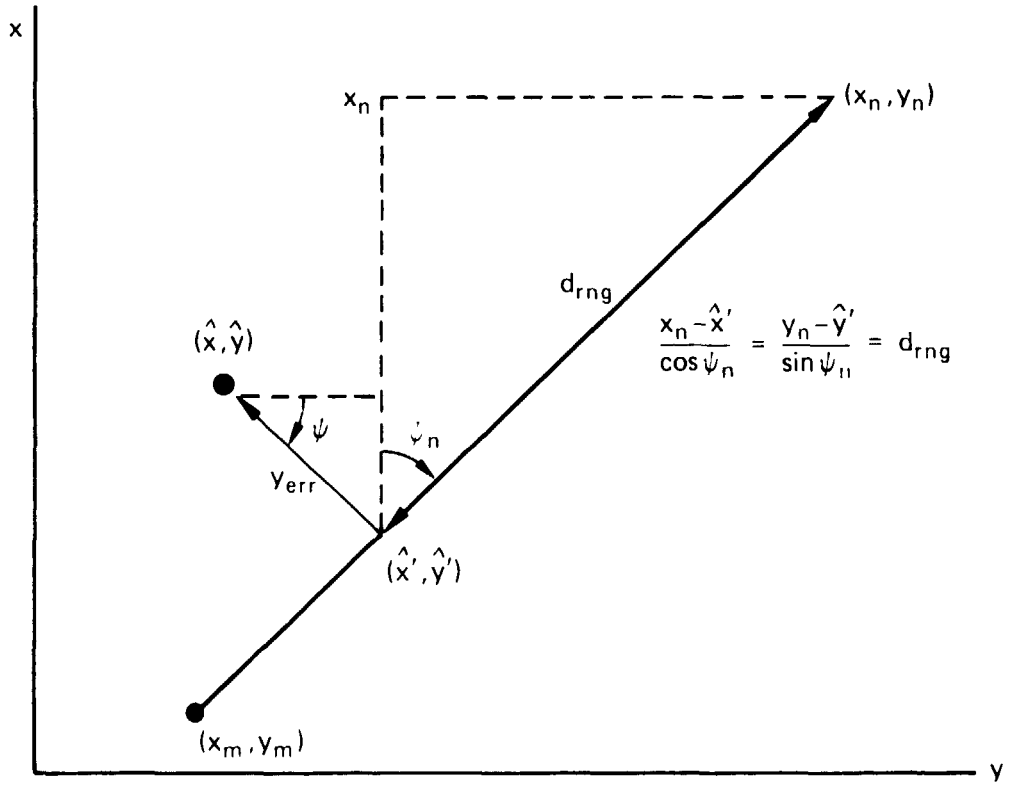

Figure A7.- Range to next waypoint geometry for straight-line segment.

Horizontal capture- In order to lead a turn between segments, the bank angle command is issued somewhat before the waypoint is reached. The decision to switch between horizontal path segments is based upon the best estimate of ground speed and range to the waypoint according to the relationship

$$KV_g \geq d_{rng} \quad , \quad K = 2.9 \text{ sec} \tag{A29}$$

where K was found experimentally to result in a smooth transition.

Vertical capture- The system switched between vertical path elements when the predicted pitch maneuver will result in a nominal normal acceleration during the transition. From figure A9 the switching range is

$$d_{rng} = R \frac{\Delta\gamma}{2} \tag{A30}$$

and further,

$$n_{acc} = \frac{V_g^2}{R} \tag{A31}$$

where R is the circular pitch maneuver radius, the acceleration $n_{acc} = 0.69$ m/sec^2, V_g is the ground speed, and $\Delta\gamma$ is the difference between flightpath angles, which is also equal to the predicted change in pitch angle during the maneuver. The transition in vertical guidance and the predicted pitch maneuver are switched when

$$n_{acc} \geq 0.69 \text{ m/sec}^2$$

or

$$\left| \frac{V_g^2 \Delta\gamma}{2 \times 0.69} \right| \geq d_{rng} \tag{A32}$$

From the above discussion, it is clear that vertical and circular captures are each initiated at different distances d_{rng} from the next waypoint. Therefore, flightpath design for the present system is limited to having either a change of flightpath angle or a change of flightpath radius at a waypoint. To complete the vertical capture maneuver, the distance d_{rng} for changing glide-slope angle must be shorter than the distances between the last and the present waypoint and between the present and the next waypoint (fig. A8). The distance d_{rng} for roll initiation is usually relatively small compared to that for glide-slope angle changes. To remove the above restrictions would result in a much more complex logic structure of the program. This concludes the description of the 3D path tracking guidance. Time-of-arrival control, the fourth dimension of the guidance problem will now be discussed.

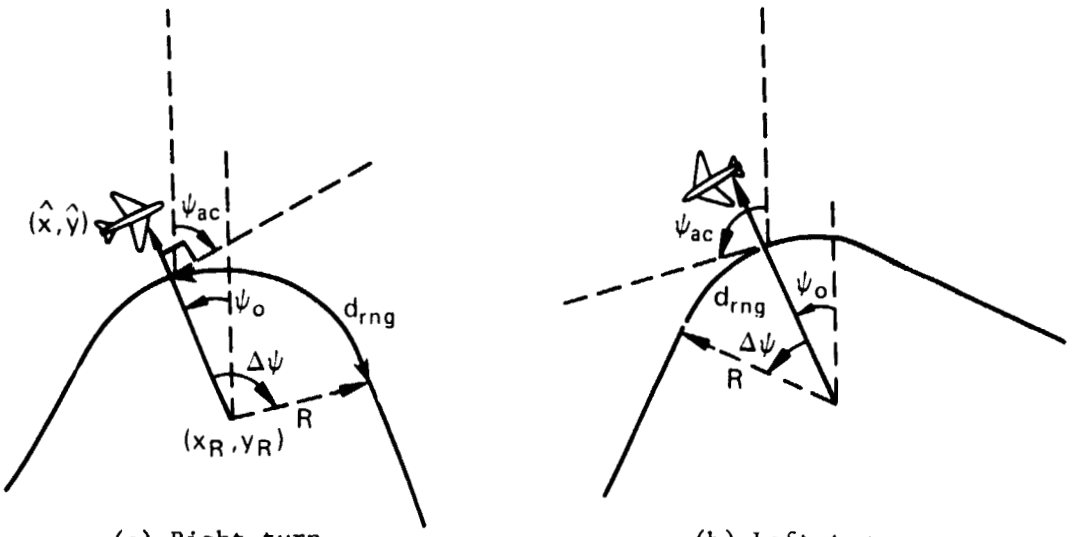

(a) Right turn. (b) Left turn.

Figure A8.- Range to next waypoint geometry for circular flightpath.

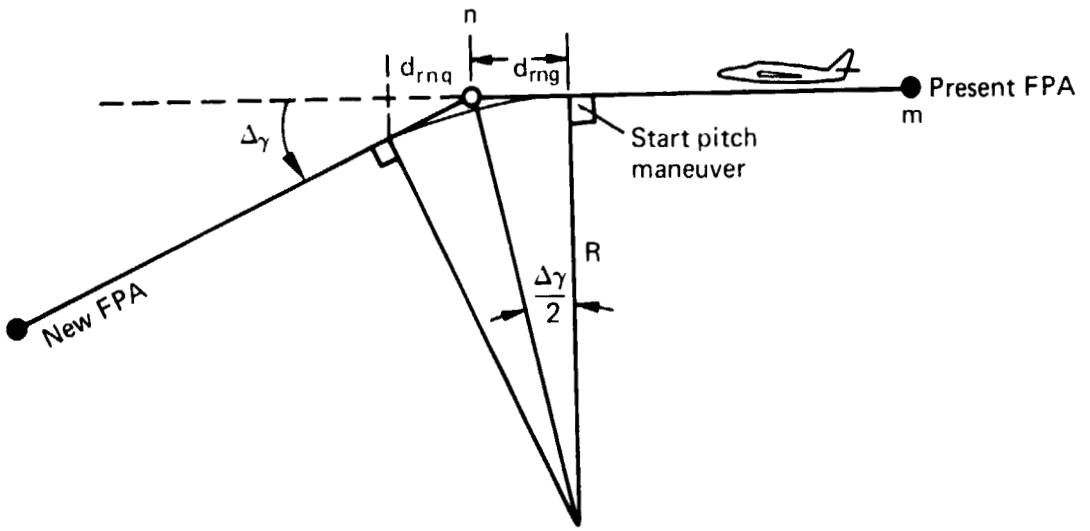

Figure A9.- Vertical capture maneuver.

Time-of-Arrival Control

The object of time-of-arrival control is to permit the aircraft to arrive at a specified waypoint within a closely defined time interval, in order to permit high-density sequencing operations for aircraft in the terminal area. The time-of-arrival control at the final waypoint is based on speed control only. Path stretching capability has not been provided. Speed control for 4D RNAV is achieved by providing an airspeed command to the aircraft speed control system.

The airspeed command V_{cref} is defined to be the sum of a prescribed nominal airspeed V_{AN} and an error which is proportional to an aircraft position error

$$V_{cref} = V_{AN} + K_6 \Delta S \quad , \quad K_6 = 0.04 \text{ sec}^{-1} \tag{A33}$$

The term ΔS is the distance along the track from the aircraft position to a moving phantom target position (fig. A3), which is positive when the phantom is ahead of the aircraft. The reference airspeed V_{cref} calculated via equation (A33) is also governed to fall between specified speed limits which are dictated by aircraft structural design safety margin and also by ATC considerations.

The generated phantom target position is the desired aircraft position. Initially, at the aircraft's arrival at the first selected waypoint, the phantom and aircraft positions coincide. The computed time it will take from the selected capture waypoint to the final waypoint is based on the aircraft flying the complete trajectory exactly at the nominal airspeed, provided the wind does not change. The arrival time is thus fixed when the aircraft passes the capture waypoint, and the time is displayed to the pilot on the MFD. For test purposes a time delay or advance can be added to the nominal flight time before engaging the 4D system by entering the number of seconds delay as WTE = --- on the STOLAND keyboard and then reinitializing the system by entering WDE = 1. This simulates late or early arrival at the first selected waypoint, which the system will try to make up by speed control.

From the foregoing discussion it is apparent that the nominal time of arrival will not be known until passing the first waypoint, nor can it be preassigned. In an operational system this would not fulfill the requirements. One solution, investigated at Ames Research Center, employs a timed, continuously recomputed, capture flightpath (ref. 9) to a selected waypoint so as to achieve the desired time of arrival.

Every 10 sec the position of the phantom aircraft is recomputed based on the latest estimate of wind velocity and direction, such that the critical waypoint arrival time will be satisfied with the aircraft flying with the least deviation from the nominal airspeed V_{AN}. Hence, the system attempts to meet the critical waypoint arrival time flying at the nominal airspeed. As long as the aircraft and the desired target position coincide, the aircraft will deviate from nominal airspeed only due to subsequent changes in the estimated wind velocity.

Calculation of the Distance Between Phantom and Aircraft

The components of ΔS- Figure 10 illustrates the notation for the distance components employed in computing the position error ΔS

$$\Delta S = d_{ng} + S_{i_A+1,i_T} + S_{i_T,T} \tag{A34}$$

The aircraft position is measured with respect to the waypoint next ahead of the aircraft, denoted as $i_A + 1$, and the phantom target position is measured with respect to the waypoint i_T which is immediately behind the target. Distances are measured in the direction of flight along the track. Desired arrival times $\{t_i\}$ at the intermediate waypoints are recomputed every 10 sec, based on the nominal airspeed V_{AN}, the latest estimate of wind velocity V_w, and distances between waypoints $\{d_i\}$. The generated phantom target position will therefore make discrete jumps resulting from these wind changes. However, it represents the best estimate of where the aircraft should be to satisfy the critical arrival time, assuming the wind to remain constant thereafter. To prevent such fast jumps, which would cause excessive throttle activity, ΔS is rate limited to 6.1 m/sec. In addition, limits on position and rate of change of the airspeed command signal V_{cref} serve to reduce jumps in the throttle command signal.

Computation of phantom target position within a path segment- The specification of the phantom target position will now be outlined. The time at which the phantom enters a flightpath segment is determined by the target time computations given in a following section.

The problem of generating the phantom trajectory is essentially that of generating a nominal ground speed V_{GN} along a specified flightpath for a given wind estimate. The nominal airspeed is specified for each waypoint so that the ground speed profile is the vector summation of the wind with the airspeed profile, where the airspeed profile between waypoints includes any nominal acceleration programs. We are interested in the solution of the following integral equation:

$$S_{i_T,T}(t) = \int_{t_{i_T}}^{t} V_{GN}\left[S_{i_T,T}(t')\right] dt' \tag{A35}$$

The integrand is ground speed, which is a function of position along the trajectory, which in turn is a function of time t'. The nominal ground speed V_{GN} is equal to the vector sum of the nominal airspeed and the wind estimate:

$$V_{GN} = \sqrt{V_{AN}^2 - V_w^2 \sin^2 \alpha} + V_w \cos \alpha \tag{A36}$$

The geometrical relationship of equation (A36) is illustrated in figure 11.

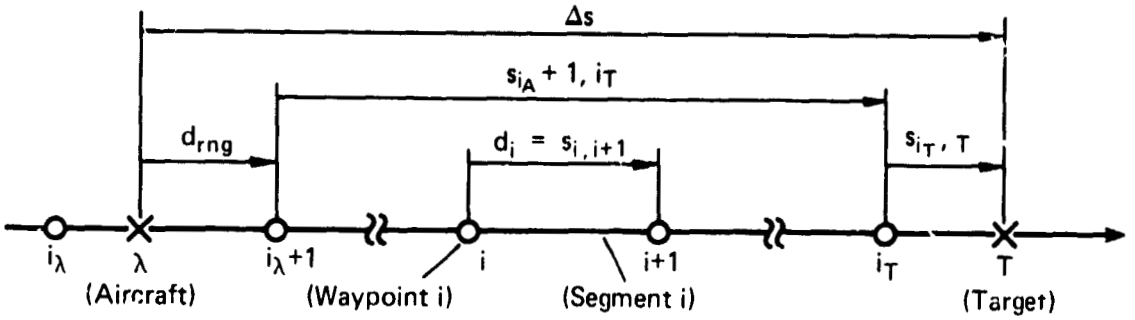

Figure A10.- Notation for distances along the trajectory.

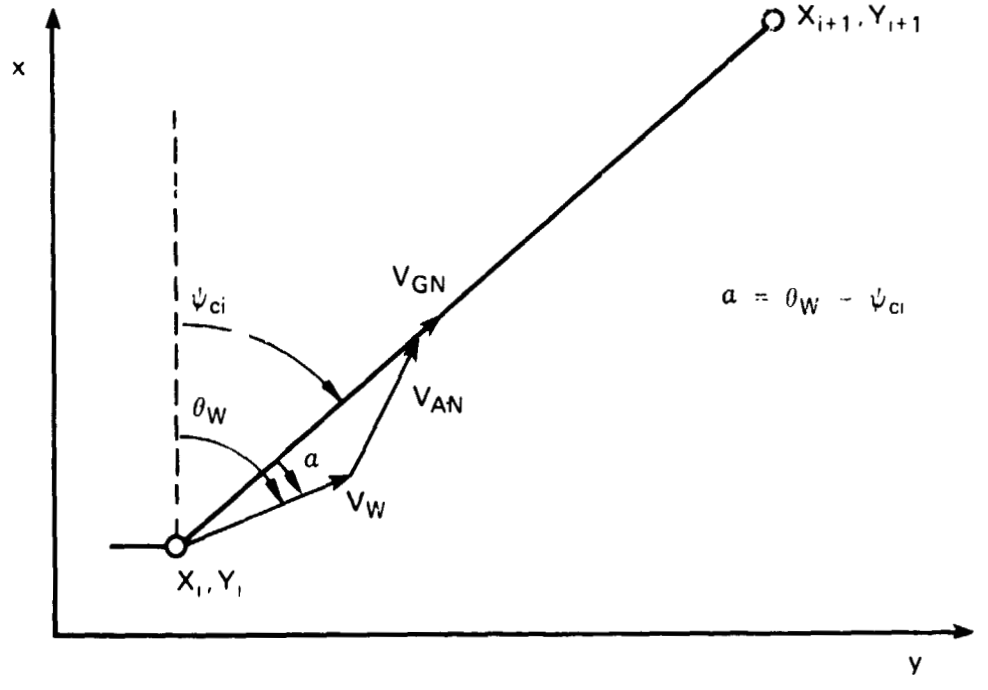

Figure A11.- Geometry of wind, airspeed summation.

For the computation of the phantom trajectory, it is assumed that

$$V_w^2 \sin^2 \alpha << V_{AN}^2 \tag{A37}$$

so that

$$V_{GN} \approx V_{AN} + V_w \cos \alpha \tag{A38}$$

(which assumes a relatively small crab angle).

The nominal airspeed V_{AN} can be expressed as a linear function of S_i, the distance along the segment i

$$V_{AN}(S_i) = V_{AN,i} + D_i S_i \tag{A39}$$

where $V_{AN,i}$ is the prescribed nominal air velocity at waypoint i, and D_i is a velocity gradient that defines a nominal acceleration program, equation (A11). Similar expressions apply to the maximum and minimum speed limits as illustrated in figure A12. To accommodate a changing wind angle α along a curved segment, let

$$\alpha(S_i) = \alpha_i - \frac{S_i}{R_i} \tag{A40}$$

where α_i is the angle of V_w with respect to the direction of the flight-path segment immediately beyond waypoint (i), S_i is the distance along the segment, and R_i is the radius of curvature of the segment with the proper sign for right or left turn. Substituting equation (A40) into (A38) and expanding gives

$$V_{GN}(S_i) = V_{AN,i} + D_i S_i + N_i \cos \frac{S_i}{R_i} + M_i \sin \frac{S_i}{R_i} \tag{A41}$$

which is valid for both straight and curved segments (fig. A13). The terms M_i and N_i are the crosstrack and the alongtrack wind components at waypoint i, respectively:

$$M_i \triangleq V_w \sin \alpha_i = -a_i V_{wx} + b_i V_{wy} \tag{A42}$$

$$N_i \triangleq V_w \cos \alpha_i = b_i V_{wx} + a_i V_{wy} \tag{A43}$$

where V_{wx} and V_{wy} are the filtered x and y runway axes components of V_w, the wind estimate.

---

[1] In the CV-340 implementation, the sign of R was not considered.

[2] In the CV-340, a_i instead of $-a_i$ was used.

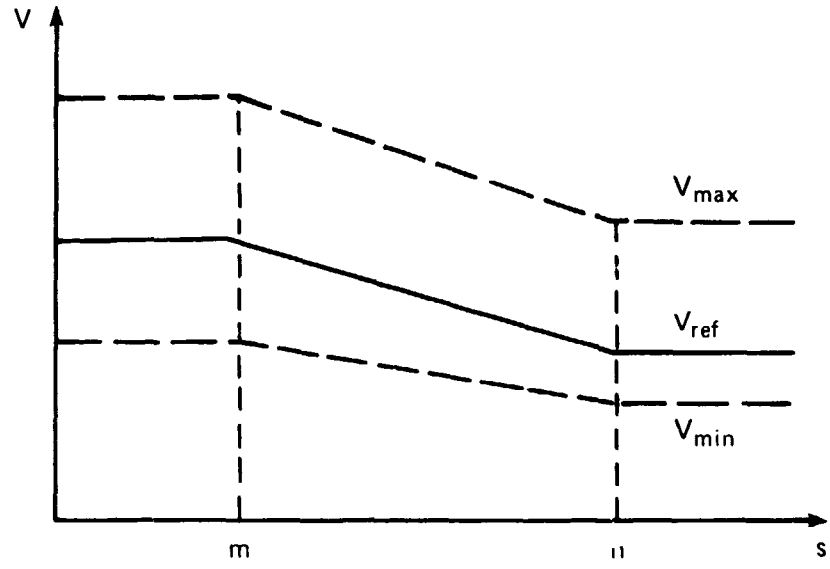

Figure A12.- Nominal airspeed and airspeed boundaries vs distance along the path.

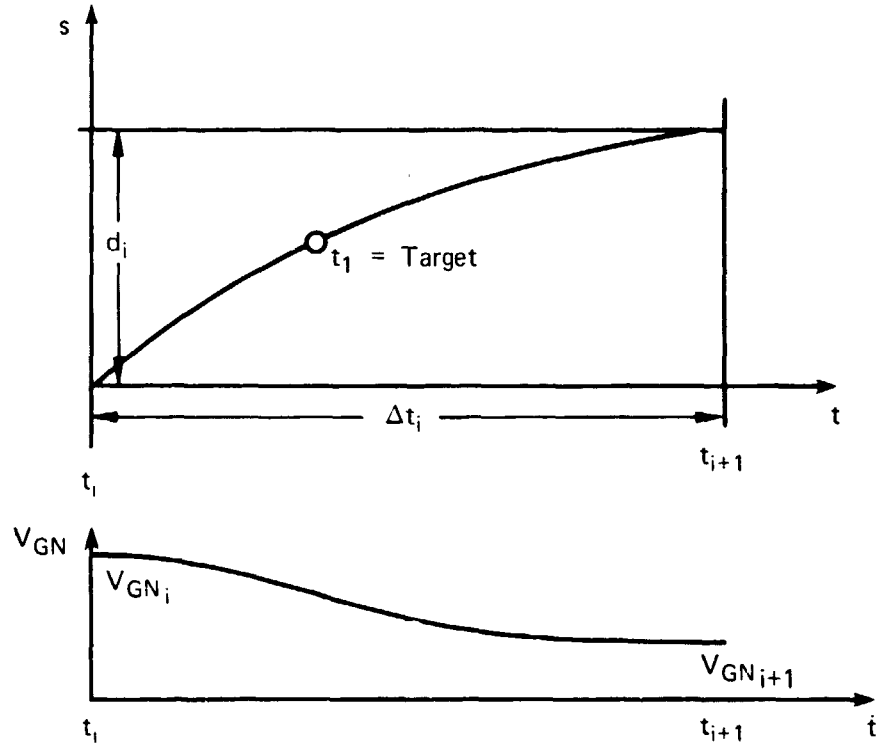

Figure A13.- Position-velocity profile with acceleration.

The terms a_i and b_i are the direction sine & cosine of the waypoint-specified trajectory (eqs. (A3) and (A4)). The expression for $V_{GN}(Si)$ given in equation (A41) could be used as the integrand of equation (A5), and the integration performed continuously in real time would yield the desired position function $S_{i_T,T}$. However, if we are willing to accept a phantom trajectory which satisfies arrival time and endpoint velocities but which may not follow the precise profile given in equation (A35), a simpler function for $S_{i_T,T}$ can be employed which has the advantage of avoiding excessive computational complexity.

$$S_{i_T,T}(t) = \left(V_{AN,i_T} + N_{i_T}\right)\left(t - t_{i_T}\right) + A_{i_T}\left(t - t_{i_T}\right)^2 + B_{i_T}\left(t - t_{i_T}\right)^3 \qquad \text{(A44)}$$

where

$$A_{i_T} = \frac{3d_i}{\Delta t_i^2} + \frac{\left(-2V_{AN,i_T} - 2N_{i_T} - V_{AN,i_T+1} - N_{i_T+1}\right)}{\Delta t_i} \qquad \text{(A45)}$$

and

$$B_{i_T} = \frac{-2d_i}{\Delta t_i^3} + \frac{\left(V_{AN,i_T} + N_{i_T} + V_{AN,i_T+1} + N_{i_T+1}\right)}{\Delta t_i^2} \qquad \text{(A46)}$$

The constants A_{i_T} and B_{i_T} are calculated from incorporating the endpoint constraints on the time and velocity in equation (A44). The parameter Δt_i, the time between waypoints i and i + 1 on the nominal groundspeed profile, is determined in the following section.

For the special case where the segment is linear and V_{AN} is constant over the segment, $A_i = B_i = 0$, and the target position becomes simply

$$S_{i_T,T}(t) = \left(V_{AN,i_T} + N_{i_T}\right)\left(t - t_{i_T}\right) \qquad \text{(A47)}$$

Since some of the parameters used in the above equations (N_i, t_i, Δt_i) are recomputed at the 10-sec wind-estimate update cycle, $S_{i_T,T}(t)$ will generally make discrete jumps at these times. Methods to reduce the undesirable effects on throttle activity arising from this computational technique are discussed in reference 10.

Arrival Time Computation

The final waypoint is designated as "critical" in that the aircraft is required to arrive there at the time which was calculated on initial path acquisition. Desired "arrival times" for the waypoints leading to the critical waypoint in order to make good this requirement are computed every 10 sec.

Arrival times $\{t_i\}$ for the waypoints leading to the critical waypoint J are obtained in terms of computed segment times Δt_i and the critical arrival time t_J as follows:

$$t_i = t_J - \sum_{j=i}^{J-1} \Delta t_j, i < J \tag{A48}$$

Arrival times are required only for the waypoints in the range

$$i_T \leq i < J \tag{A49}$$

See figure A14 for an illustration of the computation.

The time required to fly from waypoint i to waypoint i + 1 at a nominal ground velocity V_{GN} along the trajectory is

$$\Delta t_i = \int_0^{d_i} \frac{ds_i}{V_{GN}(S_i)} \tag{A50}$$

where S_i is the distance variable measured along the segment from waypoint i, and d_i is the distance between waypoints i and i + 1. The term V_{GN} was defined in the last section as the vector sum of the prescribed nominal air velocity V_{AN} and the estimated wind velocity V_w (eq. (A38)):

$$V_{GN} \approx V_{AN} + V_w \cos \alpha$$

where α is the angle of V_w with respect to V_{GN} as illustrated in figure A11.

A further justification for using the approximate expression (A38) for V_{GN} in equation (A50) is that small errors in the computation of Δt_i do not affect the time of arrival at the critical waypoint as long as it is possible to meet the arrival time within the airspeed limits. Small errors in computing Δt_i result in small deviations in ground speed from the nominal value. This has been shown to result in acceptable tolerances on time-of-arrival control.

For cases other than linear segments with constant V_{AN}, the solution of equation (A50) is approximated by rectangular egration. The expression for $V_{GN}(S_i)$ as derived in the last section is:

$$V_{GN}(S_i) = V_{AN,i} + D_i S_i + N_i \cos \frac{S_i}{R_i} + M_i \sin \frac{S_i}{R_i} \tag{A51}$$

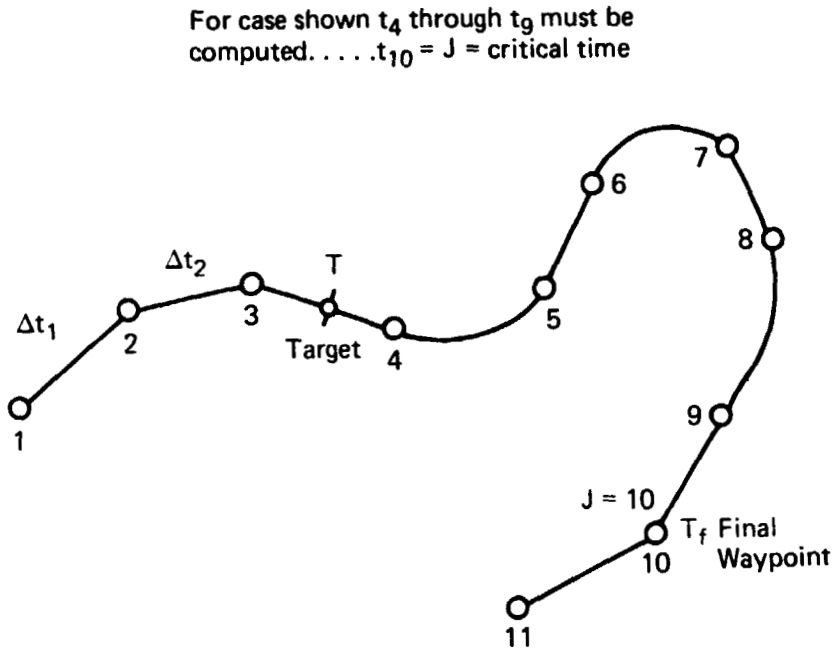

For J = 10

$$t_4 = t_{10} - \sum_{j=4}^{9} \Delta t_j$$

Figure A14.- Illustration of computation of t_i.

where $V_{AN,i}$ is a data input nominal airspeed, D_i is a velocity gradient (eq. (A11)), and N_i and M_i are computed at 10-sec intervals from updated wind estimates and constants obtained in the initialization routine (eqs. (A42) and (A43)). Therefore

$$\Delta t_i = \int_0^{d_i} \frac{ds_i}{V_{AN,i} + D_i S_i + N_i \cos (S_i/R_i) + M_i \sin (S_i/R_i)} \tag{A52}$$

For the special case where the segment is linear and V_{AN} is constant,

$$\Delta t_i = \frac{d_i}{V_{AN,i} + N_i} \tag{A53}$$

and this simplification is always employed in this case. Otherwise, rectangular integration will be employed to approximate equation (A52) as follows:

$$\Delta t_i = \Delta S_i \sum_{k=1}^{K-1} \frac{1}{V_{GN}(k\Delta S_i)} + (d_i - K\Delta S_i) \frac{1}{V_{GN}(K\Delta S_i)} \tag{A54}$$

where ΔS_i is a judiciously chosen integration increment, and K is the greatest integer less than $d_i/\Delta S_i$. For a circular segment, ΔS_i is selected to be the distance traveled in a 15° turn:

$$\Delta S_i = \frac{\pi}{12} R_i \tag{A55}$$

By thus constraining $k\Delta S_i/R_i$ to take on fixed discrete values, the sine and cosine functions in $V_{GN}(k\Delta S_i)$ can be stored in very brief look-up tables. For a linear segment (with changing V_{AN}), ΔS_i is selected to be 152.4 m.

If the aircraft is greatly behind schedule, it is either accelerating or flying at maximum permissible airspeed attempting to catch the target position. Similarly, if it is greatly ahead of schedule, it is either decelerating or flying at minimum permitted airspeed. The amount by which the aircraft is expected to be in error from the nominal arrival time due to the imposed maximum and minimum speed limits is calculated as follows for presentation on the multifunction display.

The minimum time required to get to critical waypoint J is given by

$$t_{A,J}^{min} = t_{A,i_A+1}^{min} + \sum_{i=i_A+1}^{J-1} \Delta t_i^{min} \tag{A56}$$

where t^{min}_{A,i_A+1} is the minimum time required to go to the next waypoint, and Δt^{min}_i is the minimum time required to go from waypoint i to waypoint $i+1$. An analogous expression can be written for the maximum time possible in going to waypoint J, denoted by $t^{max}_{A,J}$. The computation of Δt^{min}_i and Δt^{max}_i is identical to the computation of Δt_i described above, except that $V_{AN}(S_i)$ is replaced with $V^{max}_A(S_i)$ and $V^{min}_A(S_i)$, respectively. Both velocity functions are required to vary linearly between waypoints and thus can be expressed in terms of their values at the waypoints as for $V_{AN}(S_i)$.

The minimum time required to get to the next waypoint, $i_A + 1$, is given by

$$t^{min}_{A,i_A+1} = \int_{d_{i_A}-S_{A,i_A+1}}^{d_{i_A}} \frac{ds_i}{V^{max}_G(S_i)} \tag{A57}$$

where S_{A,i_A+1} is the distance to waypoint i_A+1 at the 10-sec computation interval, and $V^{max}_G(S_i)$ is the same as $V_{GN}(S_i)$ except that $V_{AN}(S_i)$ is replaced with $V^{max}_A(S_i)$. If segment i_A is linear and $V^{max}_A(S_i)$ is constant,

$$t^{min}_{A,i_A+1} = \frac{S_{A,i_A+1}}{V^{max}_{A,i_A} + N_{i_A}} \tag{A58}$$

In general,

$$t^{min}_{A,i_A+1} = \int_{d_{i_A}-S_{A,i_A+1}}^{d_{i_A}} \frac{ds_i}{V^{max}_{A,i_A} + d^{max}_{i_A} S_i + N_{i_A}\cos(S_i/R_{i_A}) + M_{i_A}\sin(S_i/R_{i_A})} \tag{A59}$$

which is also approximated by rectangular integration as in equation (A54), and t^{max}_{A,i_A+1} is obtained by an analogous expression.

The aircraft is expected to be able to arrive at critical waypoint J at the prescribed arrival time t_J if the remaining time $t_J - t$ lies within the range

$$t^{min}_{A,J} \le (t_J - t) \le t^{max}_{A,J} \tag{A60}$$

where t is the current real time. Therefore, if

$$t > t_J - t_{A,J}^{min} \tag{A61}$$

then the aircraft is estimated to arrive late by

$$t_{late} = t - t_J + t_{A,J}^{min} \tag{A62}$$

Similarly, if

$$t < t_J - t_{A,J}^{max} \tag{A63}$$

Then the aircraft is estimated to arrive early by

$$t_{early} = t_J - t_{A,J}^{max} - t \tag{A64}$$

The Flight Director System

The 4D RNAV system is designed for automatic operation with the pitch, roll, and speed commands driving control servos. The control servos were not installed, however, on the first test aircraft which provided the data in this report. For this reason, the 4D RNAV commands were converted to flight director commands. To complete the system description for the data reported here, the conditioning of the control law signals, described earlier and suitable for input to the flight director system, will be described next.

The pitch command, computed by the automatic control law (eq. (A16)) is first limited as an inverse function of airspeed (see fig. A15). The limited pitch command is then compared with the actual pitch of the airplane, which is washed out over 16 sec to allow the aircraft to assume new trim conditions when flightpath angle or airspeed is changed. The pitch rate sensor signal is added to the vertical reference pitch signal through a gain in order to provide damping in tracking the pitch command bar. To prevent the flight director bar from jumping when the system is engaged, the pitch angle is synchronized whenever a new guidance mode is engaged.

As shown in figure A16, the roll command output from the automatic control system is limited to 30°, filtered with a 1-sec time constant low-pass filter, and limited to a 6° per second roll rate to further reduce the effects of the navigation noise. The filtered roll command is then compared with the measured roll angle, and roll rate information is added for damping. The resulting roll error is limited and scaled for suitable presentation on the display.

For time-of-arrival control without autothrottle, a speed control flight director is required. Therefore, an error signal in the form of a black bar was displayed on the EADI, which represents the rate-limited difference between commanded and measured airspeed. For the conventional aircraft, the CV-340, this was sufficient for reasonable time-of-arrival control.

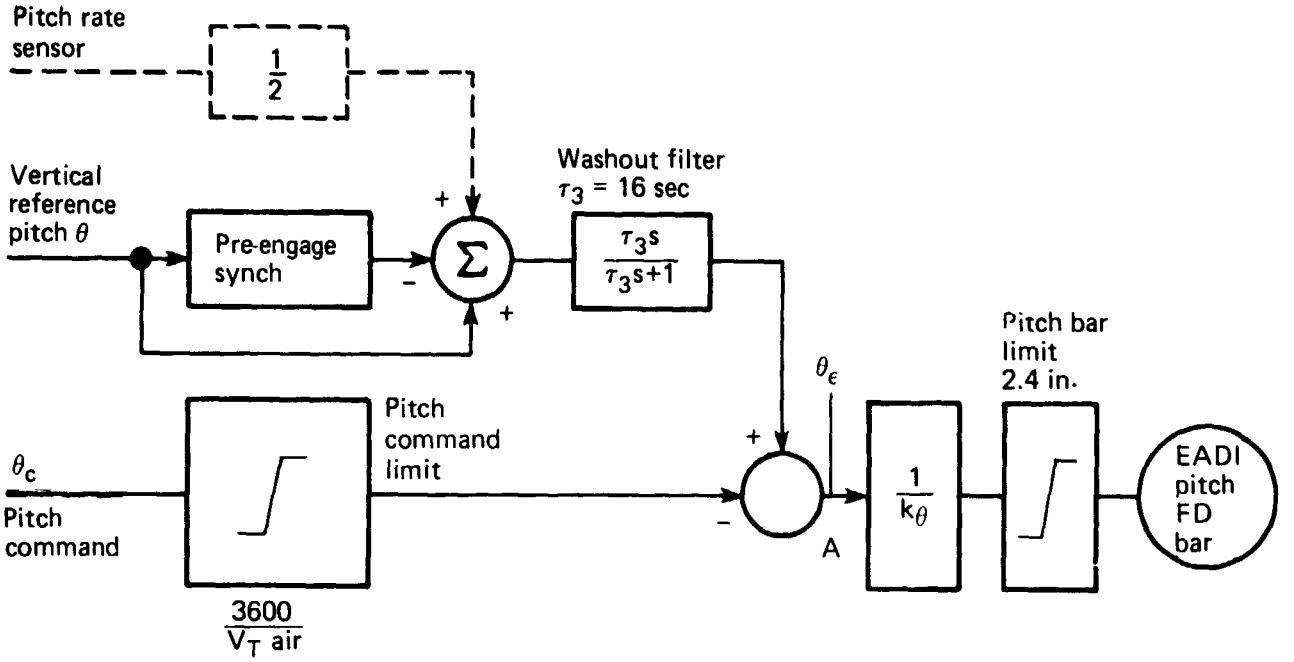

Figure A15.- Pitch flight director.

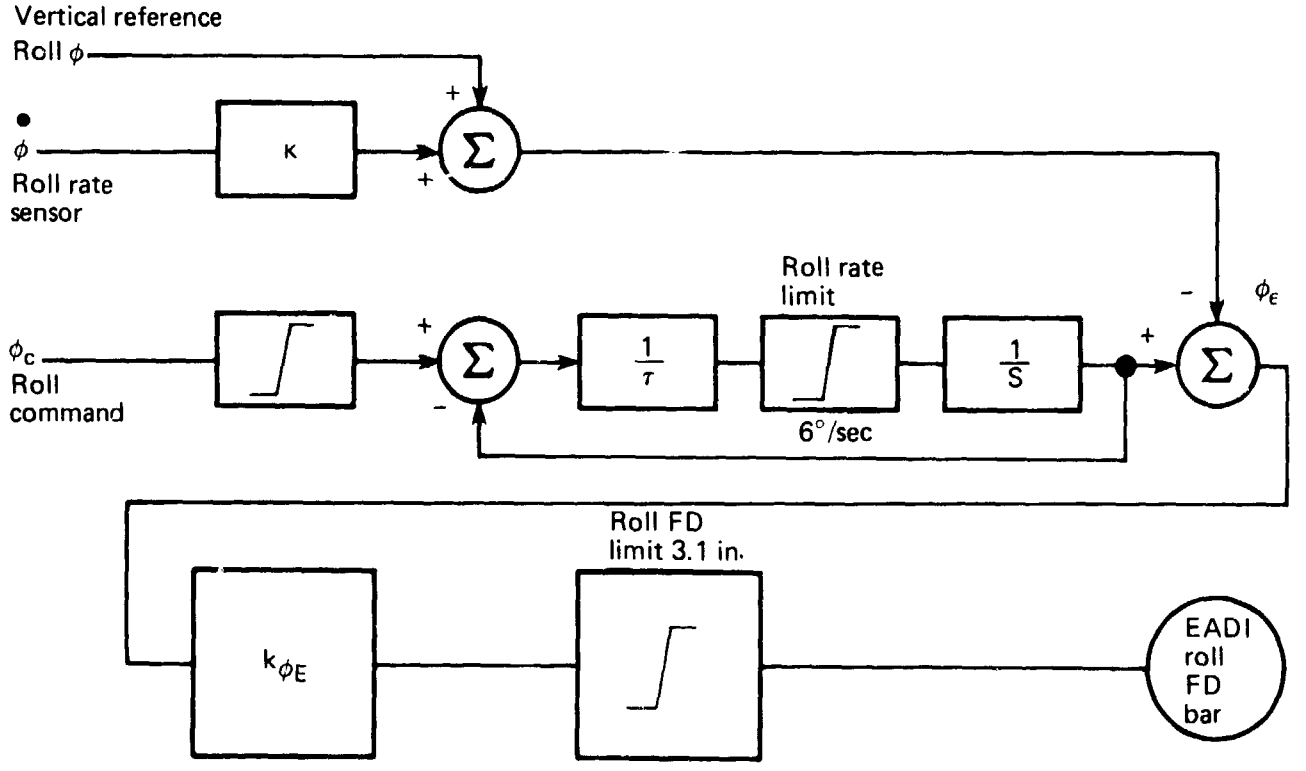

Figure A16.- Roll flight director.

APPENDIX B

NAVIGATION ERRORS IN MOVING RECTANGULAR COORDINATES

To study the interplay of navigation and guidance errors, it is convenient to express the navigation errors in the same coordinate system as guidance errors. Since guidance errors are calculated as alongtrack and crosstrack errors, the same convention is used for expressing navigation errors in this report:

The following definitions are needed (see fig. B1):

x_{NE}	positive if estimated position ahead of radar
y_{NE}	positive if estimated position to right of radar
z_{NE}	positive if estimated altitude above radar
$\bar{x}_R$, $\bar{y}_R$, $\bar{z}_R$	unit vectors defining radar coordinate frame
$\bar{x}$, $\bar{y}$, $\bar{z}$	unit vectors defining moving coordinate frame
x_R, y_R, z_R	components of reference flightpath position measured in radar coordinate frame
$\hat{x}$, $\hat{y}$, $\hat{z}$	components of estimated airplane position measured in radar coordinate frame

Derivation of the navigation error is as follows:

$$\begin{pmatrix} \bar{y} \\ \bar{x} \\ \bar{z} \end{pmatrix} = \begin{pmatrix} c\psi & s\psi & 0 \\ -s\psi & c\psi & 0 \\ 0 & 0 & 1 \end{pmatrix} \begin{pmatrix} \bar{y}_R \\ \bar{x}_R \\ \bar{z}_R \end{pmatrix} \tag{B1}$$

$$\overline{\text{N.E.}}\Big|_{x_R y_R z_R} = \overline{\text{N.E.}}\Big|_{xyz} \tag{B2}$$

Equation (B2) states that the vector navigation error in the radar frame of reference is equal to the vector navigation error in the rotating frame. Expansion of equation (B2) gives

$$(\hat{x} - x_R)\bar{x}_R + (\hat{y} - y_R)\bar{y}_R + (z_R - \hat{z})\bar{z}_R = x_{NE}\bar{x} + y_{NE}\bar{y} + z_{NE}\bar{z} \tag{B3}$$

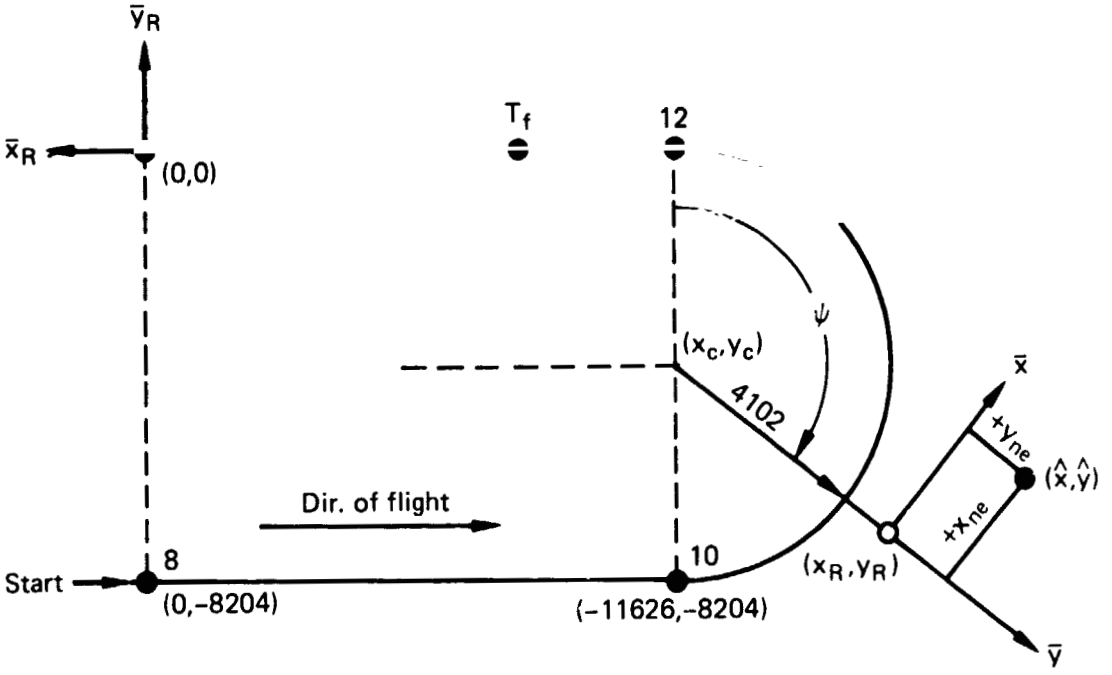

Figure B1.- Navigation error calculation geometry.

Substitution of equation (B1) into (B3) gives

$$x_{NE}\bar{x} + y_{NE}\bar{y} + z_{NE}\bar{z} = (\hat{x} - x_R)(s\psi\bar{y} + c\psi\bar{x}) + (\hat{y} - y_R)(c\psi\bar{y} - s\psi\bar{x}) + (z_{\cdot} - \hat{z})\bar{z} \tag{B4}$$

Therefore,

$$\begin{pmatrix} x_{NE} \\ y_{NE} \\ z_{NE} \end{pmatrix} = \begin{pmatrix} (\hat{x} - x_R)c\psi - (\hat{y} - y_R)s\psi \\ (\hat{x} - x_R)s\psi + (\hat{y} - y_R)c\psi \\ z_R - \hat{z} \end{pmatrix} \tag{B5}$$

Equation (B5) requires the angle ψ. For the initial straight part of the flightpath, it is 180°. For the final straight portion of the path, it is 0°. For the intermediate semicircular portion, it may be found as follows:

$$\bar{y} = \frac{(x_R - x_c)\bar{x}_R + (y_R - y_c)\bar{y}_R}{\sqrt{(x_R - x_c)^2 + (y_R - y_c)^2}} \tag{B6}$$

Substitution of $\bar{y}$ from equation (B1) into equation (B6) gives

$$c\psi\bar{y}_R + s\psi\bar{x}_R = \frac{(x_R - x_c)\bar{x}_R + (y_R - y_c)\bar{y}_R}{\sqrt{(x_R - x_c)^2 + (y_R - y_c)^2}} \tag{B7}$$

Therefore,

$$s\psi = \frac{x_R - x_c}{\sqrt{(x_R - x_c)^2 + (y_R - y_c)^2}} \tag{B8a}$$

$$c\psi = \frac{y_R - y_c}{\sqrt{(x_R - x_c)^2 + (y_R - y_c)^2}} \tag{B8b}$$

or

$$\tan\psi = \frac{x_R - x_c}{y_R - y_c} \tag{B9}$$

Equation (B8) gives values for $s\psi$ and $c\psi$ directly but requires a square root, whereas equation (B9) requires an ATAN and then taking the sine and cosine. The results are tabulated on the following page.

Restrictions	ψ	Navigation error	Track distance
$x_R < 0$ $x_R > -11626$ $y_R < -4102$	$\psi = 180°$	$x_{NE} = x_R - \hat{x}$ $y_{NE} = y_R - \hat{y}$ $z_{NE} = z_R - \hat{z}$	$s = -x_R$
$x_R < -11626$	$\psi = \text{ATAN}\left(\frac{x_R - x_c}{y_R - y_c}\right)$	$x_{NE} = (\hat{x} - x_R)c\psi - (\hat{y} - y_R)s\psi$ $y_{NE} = (\hat{x} - x_R)s\psi + (\hat{y} - y_R)c\psi$ $z_{NE} = z_R - \hat{z}$	$s = 11626 + 4102 (\pi/2 + \psi_1)$ where $\psi_1 = \text{ATAN}\left[\frac{y_R - y_c}{-(x_R - x_c)}\right]$
$x_R < 0$ $x_R > -11626$ $y_r > -4102$	$\psi = 0°$	$x_{NE} = \hat{x} - x_R$ $y_{NE} = \hat{y} - y_R$ $z_{NE} = z_R - \hat{z}$	$s = 36139 + x_R$

REFERENCES

1. Civil Aviation Research and Development Policy Study — Report. NASA SP-265, 1971. (Also available as DOT TST-10-4.)

2. Civil Aviation Research and Development Policy Study — Supporting Papers. NASA SP-266, 1971. (Also available as DOT TST-10-5.)

3. Quigley, H. G.; Innis, R. C.; and Grossmith, S.: A Flight Investigation of the STOL Characteristics of an Augmented Jet Flap STOL Research Aircraft. NASA TM X-62,334, 1974.

4. Neuman, F.; Watson, D.; and Bradbury, Peter: Operational Description of an Experimental Digital Avionics System for STOL Airplanes. NASA TM X-62,448, 1975.

5. Neuman, Frank; and Warner, David N., Jr.: A STOL Terminal Area Navigation System. NASA TM X-62,348, 1974.

6. Lee, Homer; Neuman, Frank; and Hardy, Gordon: 4D Area Navigation System Description and Flight Test Results. NASA TN D-7874, 1975.

7. Smith, D. W.; Neuman, F.; Watson, D. M.; and Hardy, G. H.: A Flight Investigation of a Terminal Area Navigation Concept for STOL Aircraft. NASA TM X-62,375, 1974.

8. Neuman, Frank; and Lee, Homer Q.: Flight Experience with Time-of-Arrival Control for STOL Aircraft in the Terminal Area. AIAA Paper 75-1126, Aug. 1975.

9. Adams, Glen D.: Evaluation of STOL Modular Instrument Landing System (MODILS). Department of Transportation, FAA Rep. FAARD-72-4, 1972.

10. Report of Department of Transportation Air Traffic Control Advisory Committee, Dept. of Transportation, Washington, D.C., Dec. 1969.